Synthesis of Free Organotin (IV) Compounds Containing Nonsteroidal Anti-Inflammatory Drugs and their Immobilisation into Mesoporous Silica Nanoparticles

Master Thesis

for attaining the academic degree of

Master of Engineering (M.Eng)

submitted to

Merseburg University of Applied Sciences

by **Til Becker**

February 2022

First Referee: Prof. Dr. Dr. h.c. Goran Kaluđerović

Second Referee: Prof. Dr. Dr. h.c. mult. Evamarie Hey-Hawkins

Acknowledgement

Statement of Authorship

I hereby declare that I wrote this master thesis by myself without unauthorized external assistance, unless otherwise acknowledged in the text. All verbatim and referenced passages and all sources of information have been quoted and indicated.

This thesis has not been submitted for any other degree.

 Leipzig, 18.02.2022

Signed in, date

Signature

Table of Contents

List of Abbreviations

Acfa – 4-*O*-acetylated ferulic acid

BJH – Barrett, Joyner, and Halenda

COX – cyclooxygenase

CTAB – cetyltrimethylammonium bromide

DCM – dichloromethane

DFT – density functional theory

dH$_2$O – distilled water

EDX – energy dispersive X-ray spectroscopy

ESI-MS – electrospray ionisation mass spectrometry

EPR – enhanced permeability and retention

fa – ferulic acid

fen – fenoprofen

IUPAC – International Union of Pure and Applied Chemistry

MCM-41 – Mobil Composition of Matter No. 41

MSNs – mesoporous silica nanoparticles

NMR – nuclear magnetic resonance

NSAIDs – nonsteroidal anti-inflammatory drugs

PG – prostaglandin

PGG$_2$ – prostaglandin G$_2$

RES – reticuloendothelial system

SAXS – small-angle X-ray scattering

SBA-15 – Santa Barbara Amorphous-15

SEM – scanning electron microscopy

TEA – triethylamine

TEOS – tetraethyl orthosilicate

THF – tetrahydrofuran

List of Figures

Appendix

List of Tables

1. Introduction

1.1. General introduction

Around 60 years ago, the inhibiting effect of cisplatin (*cis*-diamminedichloridoplatinum(II)) was discovered by *Barnett Rosenberg* during an investigation of cell division in *Escherichia coli.*[1] Using platinum electrodes to generate an electric field, he observed stagnation in cell viability.[1] Later, he discovered that the electrolysis product from the platinum electrode was responsible for the inhibition of cell division and not the electric field. This moment led to "the birth of medicinal inorganic chemistry".[2] In 1978 U.S. Food and Drug Administration approved cisplatin for treatment of testicular cancer.[2] Until today, cisplatin is one of the most commonly used agents for chemotherapeutical treatments.[2,3] Cisplatin provides high cytotoxicity and is used to treat various types of cancer.[4] It cross-links with DNA causing irreversible damaging, that prevents DNA replication and leads further to apoptosis.[4] During chemotherapy with cisplatin, several side effects can occur, due to DNA binding with healthy tissues. One common side effect is nephrotoxicity, which can cause renal failure.[4] Furthermore, resistance mechanisms of cancer cells against cisplatin are reported, leading to increased interest in the development of new metal-based drugs.[2,4] Several studies suggest high cytotoxic activity of organotin(IV) compounds, making them good candidates for potential anticancer agents.[3,5,6]

Up to now, the low bioavailability and system damaging side effects, prevent their usage as effective anticancer drugs in present therapeutic aspects. To improve the bioavailability, nanoparticles can be used as drug delivery systems to enhance the solubility of the anticancer drugs and protect them from biodegradation.[2,7,8] Among them, mesoporous silica nanoparticles (MSNs) provide prosper potential with adjustable properties, like shape, size and pore appearance.[8,9] MCM-41 and SBA-15 are most widely used MSNs which exhibit hexagonally ordered pores with specific surface areas up to 1000 m²/g.[10,11] These nanoparticles have high biocompatibility, non-toxic behaviour and were successfully used as drug delivery systems, where the drug-loaded MSNs showed increased antitumor activity compared to the free drugs.[12,13]

1.2. Mesoporous silica nanoparticles

Due to the drawbacks of the chemotherapeutical drugs such as their short half-life, off-target action and minor biocompatibility, mesoporous silica nanoparticles have emerged as outstanding carriers for drug therapy.[9,13] Possibility of tuning specific surface area, particle size, shape and pore properties and moreover high biocompatibility of MSNs make them very attractive vehicles.[7,9,14] MSNs can be synthesised through a sol-gel process via a modified Stöber synthesis.[7,9,14] As shown in Figure 1, a micelle forming precursor is dissolved in pure water where single spherical micelle formations arrange into hexagonal assemblies.[7,8] For this step cetyltrimethylammonium bromide (CTAB) is an often used surfactant.[7,9,14]
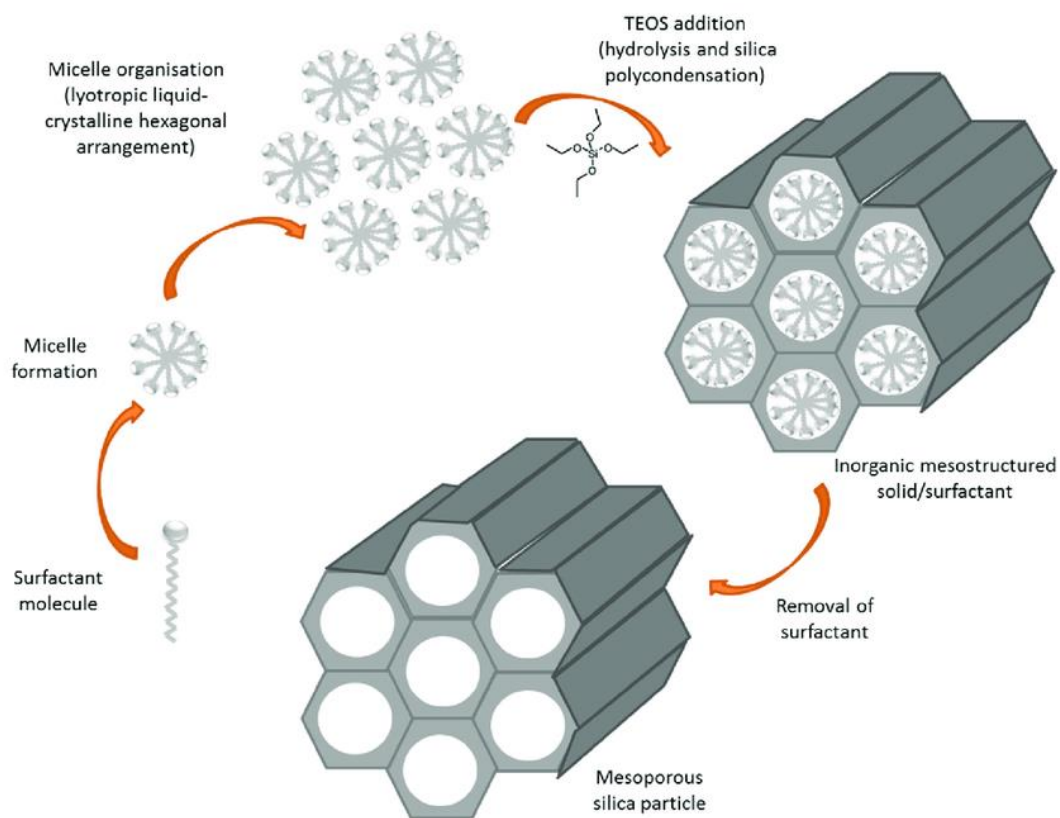
Figure 1: Schematic procedure for the synthesis of MSN [8]

Under alkaline conditions, a silica species, e.g. tetraethyl orthosilicate (TEOS), is added to the solution.[14] The silica species condensate on and around the micelle template forming silica walls and growing into an inorganic solid silica structure.[14] During this step, micelle concentration, temperature, pH and stirring speed can define the shape and size of the pores and particles.[7,9,14] After the solid silica structure is completely formed, the template inside of the structure has to be removed.[7,9,14] The removal can be managed via washing with ethanol and water followed by calcination. The most common particles MCM-41 and SBA-15 provide

spherical and rod-shaped particles, respectively.[7,10] In general, the size of the obtained MSNs can vary from 20 nm up to 1000 nm.[9,15,16]

Although the interaction between MSNs and targeted cells or biological systems is influenced by many properties, such as particle size, shape and porosity, the general uptake of nanoparticles in cells proceeds via endocytosis.[7,14] Endocytosis can be regulated by clathrin-dependent or clathrin-independent uptake.[14] Both ways result in the uptake of the particles into the cells as endosome, where the degradation of the particle is initiated.[14] Studies suggest that nanoparticles with different sizes interact differently. For instance, circulation time in bloodstream is longer for small particles, leading to possible haemolysis.[7,16] MCM-41 nanoparticles with same Brunauer-Emmett-Teller (BET) surface, but different particles sizes, 25 to 225 nm, were examined with respect to their interaction with red blood cells.[17] It has been reported that interaction was higher for small particles or for higher dosages and size dependent interaction only applies for long-range ordered pores.[17] In an *in vivo* study with mice, the distribution of MSNs was traced. Particles with 80, 120, 200 and 360 nm were given to mice intravenously and it could be observed that larger particles accumulated more in organs such as liver and spleen and to a lesser extend heart and lung, compared to the smaller ones.[18] According to the early capture, degradation of larger particles was faster than for smaller particles.[18] Despite their accumulation, no toxic and inflammatory effects were detected.[18] Another *in vivo* study reported similar results. *Lu et al.* injected intravenously 100-130 nm large particles (50 mg/kg) in mice twice per week for 14 days, resulting in a mild liver transaminase for one mouse out of two.[12] Animals which received a higher dose (100 mg/kg) showed no abnormalities upon treatment. Furthermore, long-term toxicity investigation has been carried out where mice got an intraperitoneal injection twice per week for two months and the same results have been found.[12] Additionally, excretion of 94.4% of 1 mg injected MSN within four days was observed in a mouse.[12] Phagocytes filter particles bigger than 100 nm and are mainly located in liver, spleen and lymph nodes.[14,17] Phagocytes as part of the reticuloendothelial system (RES) circulate in the bloodstream and engulf foreign particles.[19] It is not unusual that accumulation of MSNs takes place in liver, as part of metabolism, and in spleen, as part of the RES. Larger particles get trapped more easily by the immune system which may reduce their targeting. However, due to complex interplay of MSNs, their uptake and circulation has to be investigated *in vivo* in more details in order to elucidate influence of the particle size, shape and specific surface area.

Due to shape and pore dependent interaction with red blood cells, MSNs exhibit high biocompatibility *in vivo* and despite their accumulation, no major toxicity or abnormalities have been reported so far, making them beneficial drug delivery systems. The application of many drugs is limited because of their low solubility and stability in aqueous solutions preventing good bioavailability and consequently, effective therapeutic utilisation.[7,13] The usage of MSN can be beneficial for overcoming these issues. When such drugs are loaded into the MSN, they are protected from decomposition. Use of MSNs may also prevent multidrug resistance.[7] *Beck* summarises that loaded MSNs can channel the drugs into malignant cells.[7] This is beneficial taking in consideration that overexpression of P-glycoprotein plays an important role in removal of the drugs out of the cell.[7] Further, multiple loading of the nanoparticles may transport both drug and oligonucleotides that can overcome multidrug resistance.[7]

There are two ways to target specific cells: passive and active targeting.[8,9,14] Passive targeting of cancer cells can be achieved due to the enhanced permeability and retention (EPR) effect of the malignant tissue.[7,8] Malignant cells provide an abnormal, increased proliferation with the ability to spread and therefore, require more oxygen and nutrients.[14] Consequently, they have an especially high production of new blood vessels with gaps between endothelial cells, allowing bigger nanoparticles to reach these cells, see Figure 2.[8,9,14]
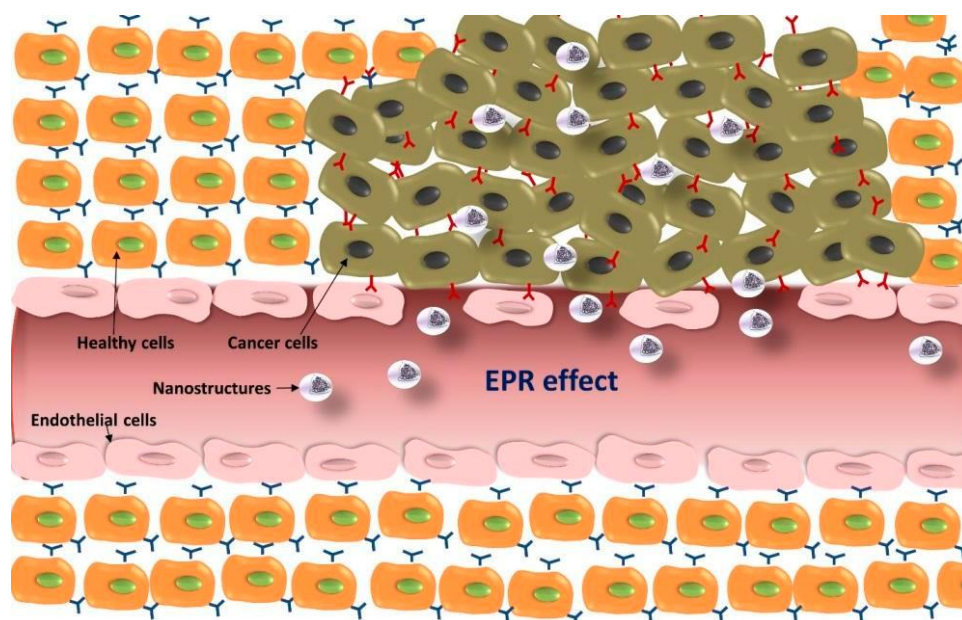
Figure 2: Schematic depiction of nanoparticles reaching malignant cells due EPR effect [8]

While in the healthy tissues the pore sizes are ca. 25 nm, the lack of endothelial cells allows the nanoparticles to leave blood vessels and accumulate at malignant cells (cut-off 380 to 780 nm). Without an efficient lymphatic drainage around malignant cells, the EPR effect can be used to

accumulate bigger particles without being cleared.[8,14] That allows the accumulation of particles up to 780 nm.[8] Thus, it increases the local impact of drug-loaded MSNs at targeted cells and decreases exposure on the whole system at the same time. All of this point out that new promising therapeutic strategies are possible.[7,8,13] For instance, *Lu et al.* could show *in vivo* that drug-loaded nanoparticles accumulated preferably in tumor tissues.[12]

However, the possibility of passive targeting therapy depends on the cancer type and it cannot be applied, for example in cancers like leukaemia when the malignant cells are circulating through the blood system.[7,8,14] Using receptor specific ligands such as peptides or whole antibodies on the surface of the MSNs, a selective binding of the nanoparticles to the receptor-expressing cells can be achieved, inducing a receptor based endocytosis at the target cell.[7–9,12,14] For instance, folate receptors are overexpressed on many tumor cells.[14] There, several successful investigations for active targeting are reported.[8,14] Furthermore, via surface modification it is possible to use ligands, that inhibit the uptake by an untargeted cell.[14]

1.3. Nonsteroidal anti-inflammatory drugs

1.3.1. General

Nonsteroidal anti-inflammatory drugs (NSAIDs) are used to reduce pain and inflammation and are among the most prescribed medications every year.[20] Furthermore, they have antipyretic properties.[20,21] The application can vary from muscle pain, pyrexia, migraines to arthritis, gout and acute trauma cases.[22] Based on their selectivity or their chemical structure, they are divided into several groups.[22,23] With regards to their chemical structure, they are classified into salicylates, acetic acids, propionic acids, fenamic acids, enolic acids and ketones.[24] The mechanism of NSAIDs consists of an inhibition of the cyclooxygenase (COX) enzyme, which is involved into synthesis of prostaglandins (PG). These prostaglandins are important inflammation mediators.

There are two isoforms of the enzyme: COX-1 and COX-2.[20,22–25] COX-1 is constitutively expressed in the body and is involved into maintaining of gastrointestinal mucosa lining, kidney functions and platelet aggregation.[22] It is necessary for gastric mucosal integrity via anti-thrombogenic and cytoprotective behaviour.[22,25] It has a housekeeping effect by synthesising compounds, which regulate normal cell activity.[24] The second isoform COX-2 is inducible expressed by inflammatory effects and is involved in inflammation, pain and fever.[22,23] Reports have shown, that COX-2 and its expression are also linked to tumor genesis.[26] Cyclooxygenase first catalyses arachidonic acid into the endoperoxide prostaglandin G_2 (PGG_2) with a COX

5

active site. The second active site of cyclooxygenase is peroxidase active, converting PGG_2 into other main inflammatory mediators.[25] An overexpression of COX-2 and consequently synthesis of prostaglandin E_2 is associated to increased angiogenesis of cancer cells.[26] Prostaglandin E_2 can stimulate cancer progression and may inhibit apoptosis in tumor cells.[26] It has been reported that in COX-2-knockedout mice, growth of cancer cells is inhibited.[27]

With focus on their selectivity, NSAIDs are classified into nonselective and selective ones, especially COX-2 selective NSAIDs.[20,23–25] Nonselective NSAIDs inhibit both COX-1 and COX-2. Because of the important role of COX-1, inhibition of it leads to gastrointestinal and platelet side effects, like gastrointestinal bleeding, perforation, abdominal pain and renal problems.[23,24] Some of the nonselective NSAIDs are aspirin, ibuprofen, naproxen, fenoprofen and ketorolac.[24] Due to these induced side effects, inhibition of only COX-2 is intended and therefore COX-2 selective inhibitors were developed. Representatives of this class of so-called coxibs are celecoxib and rofecoxib..[23–25] These drugs still inhibit COX-1 but have less effect on it in comparison to inhibition of COX-2. Their COX-2 selectivity is given by and COX-2/COX-1 inhibition ratio. The higher the ratio, the better the specific therapeutic effect and the lower the inhibition of COX-1 is achieved.[23,26] COX-2 selective NSAIDs also cause some side effects. Abdominal pain, a risk of gastrointestinal bleeding, perforation and increased blood pressure are related with this class of compounds.[23,24] Using NSAIDs in cancer therapy may lead to synergetic effects due to anti-inflammatory action and COX-2 and consequently tumor angiogenesis inhibition. Nevertheless, the usage und furthermore the field for NSAIDs as possible cancer therapy will be increased.[23,24]

1.3.2. Fenoprofen

Fenoprofen (fen), 2-(3-phenoxyphenyl)propanoic acid or its trade name Nalfon, is a drug which is used for postoperative pain.[28] For this purpose it is prescribed in countries like Austria, France, UK and USA.[28] It belongs to the group of NSAIDs, therefore it operates by inhibiting cyclooxygenase to prevent prostaglandin synthesis.[28] Fenoprofen has isopropyl moiety making it structurally similar to other common used NSAIDs like ibuprofen, flurbiprofen and naproxen, see Figure 3.[10,28]
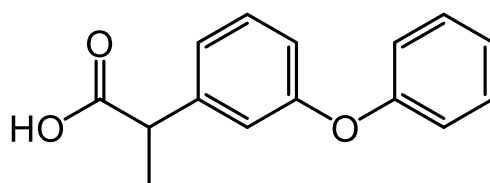
Figure 3: Structure of fenoprofen (fen)

Fenoprofen itself shows modest antiproliferative activity, but cytotoxic effects could be increased in fen amide derivates.[29] Nevertheless, inflammation can produce DNA-damaging and inflammatory cells are associated with cancer development and growth.[30]

Due to its lipophilicity character, fenoprofen, and other similar NSAIDs, must be used in high dosages to reach good bioavailability, causing more side effects as well.[31] Approaches based on the organotin(IV) containing NSAIDs can achieve the anti-inflammatory and antiproliferative effects.

1.4. Ferulic acid

Ferulic acid (fa), (2*E*)-3-(4-hydroxy-3-methoxyphenyl)prop-2-enoic acid, is an antioxidant, common in nature.[32,33] The *trans* isomer predominates up to 90% of all phenolic acids and can be found in fruits, vegetables, corn and flour.[32] It is part of the biosynthesis of lignin and plays the role as antioxidant in other biopolymers.[32,33] As showed in Figure 4, ferulic acid consists of a phenolic nucleus with an unsaturated carboxylic moiety.
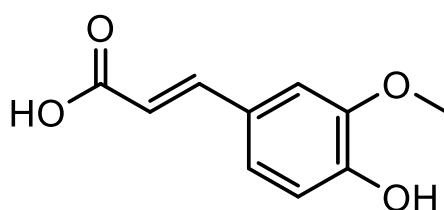
Figure 4: Structure of ferulic acid (fa)

Free radicals may induce a chain reaction inducing oxidative stress. If a radical attacks the fa, the hydroxyl group gets deprotonated, leading to a radical of the ferulic acid itself.[32] The structural characteristics of antioxidants make it possible that the radical chain reaction is stopped, by a stabilised conjugation. The radical is stabilised through conjugation between the side chain and phenoxy group, see Figure 5.
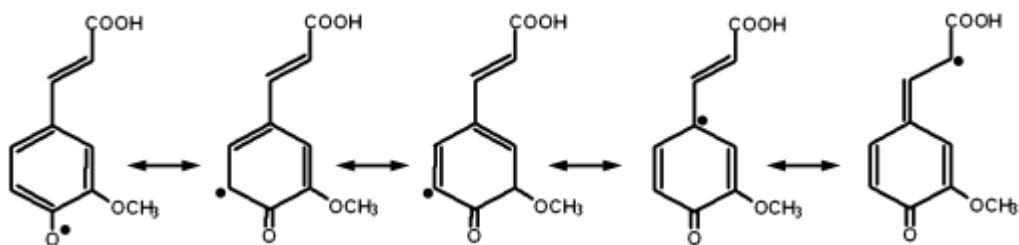
Figure 5: Ferulic acid radicals [32]

In addition to the antioxidant activity, fa exhibits also other properties potentially beneficial in therapy. Fa shows antimicrobial activity, inhibiting gastrointestinal microflora, e.g. *Escherichia coli.* Furthermore, it inhibits reactive oxygen species induced by viruses, which makes fa attractive for food and cosmetic industries.[33] Another therapeutic activity is the anti-inflammatory effect. It has been reported that fa and its derivatives decrease levels of prostaglandin E2.[32] *Nile et al.* screened several fa derivatives for their anti-inflammatory activity against two pro-inflammatory cytokines and compared them with dexamethasone, a common anti-inflammatory drug. The results showed comparable anti-inflammatory activity.[34] Same authors postulate that fa may inhibit reactive oxygen species leading to the pro-inflammatory effect. Furthermore, good COX-2 inhibiting properties for some fa derivatives were reported.[34] In addition, fa and some other phenolic acids, provide anticancer effects by inducing apoptosis.[32] *Kempa et al.* reported an anticancer activity against human breast cancer due to antiproliferative and apoptotic effects of phenolic acids, among them fa.[35]

These properties make fa an attractive ligand for the development of new potential cytotoxic drugs and therefore, it is chosen for this study.

1.5. Organotin(IV) compounds

Nowadays, cisplatin still is one of most commonly used cytostatic agents in cancer treatment.[2,3] *World Health Organization* categorized cisplatin in "model list of essential medicines" of 2021 for head and neck, ovarian and testicular cancers.[36] When cisplatin reaches the cell where chloride concentration in cytoplasm is less than 100 mM, hydrolysis of the compound into mono- and di-aqua under elimination of chlorido ligand occurs.[2] These hydrolytic products then bind to DNA bases guanine and adenine, leading finally to apoptosis. Only around 1% of the drug actually reacts with DNA.[2] The low concentration of active species in target cells as well as the multidrug resistance, reduces the efficacy of the cancer treatment and leads to application of high doses associated with more unwanted side effects.[2,3] A number of metal-based drugs

has been developed and investigated, but cisplatin and its derivatives carboplatin and oxaliplatin remain as important drugs for cancer treatment, used in around 50% of chemotherapies.[2]

Among non-platinum based metalorganic dugs, organotin(IV) compounds gain interest.[37] Organotin(IV) compounds are bioactive and as such are used in agriculture as biocides or in paint for ship hulls.[38,39] Once expressed to marine systems, they accumulate in organisms and due to sexual abnormalities assumed as endocrine-disrupting chemicals leading to imposex.[39] Especially triphenyltin(IV) and tributyltin(IV) compounds are lipophilic and have high potential for bioaccumulation.[39] Nevertheless, they revealed high cytotoxicity and can overcome multidrug resistance with indications that organotin(IV) carboxylates are more effective than cisplatin.[37,40] *Amir et al.* reported on anticancer studies with organotin(IV) carboxylates where, depending on organotin(IV) derivate and ligand, different activities against several tumour cells were shown.[37] In another study, it was presented that some tin(IV) compounds had promising activity against lymphocytic leukaemia in mice, but were inactive against the solid tumours, confirming the differential interaction of these compounds.[6] Therefore, both the tin(IV) moieties and the ligand influence the bioactivity and cytotoxic activity.[6,37] Despite dependencies on cancer cells, higher cytotoxic activities have been reported for diphenyltin(IV) moieties and dibutyltin(IV) moieties, but the mechanism of action remains unknown.[6] Yet, it has been confirmed that for triphenyltin(IV) species, π-π interactions with DNA base pairs occurs and it is suggested that apoptosis is responsible for the anticancer action.[6] *Yusof et al.* review that tin(IV) compounds inhibit "protein complexes (F_1F_0 ATP synthases), membrane-associated functions, macromolecular synthesis, protein synthesis and DNA replication" where major inhibition sites have to be understood.[6] Triorganotin(IV) compounds provide highest toxicity, but underwent disproportionation in solution and by that, diorganotin(IV) compounds seem to be best cytotoxic agents with reported higher cytotoxic action than for standard drugs for specific cancers.[6] The limited bioactivity of triorganotin(IV) compounds seems to be due to their high lipophilic character leading to low bioavailability. Among organotin(IV) compounds, triphenyltin(IV) and tributyltin(IV) derivates with carboxylato ligands showed highest cytotoxicity against human tumor cells.[5] A recent study presented novel triphenyltin(IV) carboxylates and examined their cytotoxic activity. *Pantelić et al.* tested these compounds against three different cancer cell lines and observed remarkable activity. From the obtained IC_{50} values is it clearly shown their superior activity with respect to cisplatin, ranging from 26 to 119 times.[41]

1.6. MSN as drug carriers for organotin(IV) compounds

Despite the promising properties of the triorganotin(IV) carboxylates, their application as anticancer agents might be limited due to the lipophilic character resulting in low bioavailability. With the usage of MSNs as drug carriers this problem can be overcome and the bioavailability of the active drug can be enhanced. Recent studies with organotin(IV) loaded MSNs reveal high cytotoxic effects with low concentrations. *Bulatović et al.* studied the anticancer activity of (hexanol-1-ol)triphenyltin(IV) loaded into functionalised rod shaped SBA-15 nanoparticles with the size 720×460 nm.[42] They investigated the impact of loaded MSN onto B16 melanoma cells *in vitro*. The pure organotin(IV) compound as well as the immobilised compound were tested on cellular viability of B16 cells, resulting in much higher activity for loaded particles at concentrations, where the free tin compound had no impact on the tumor cell viability.[42] Results obtained from *in vivo* tests in mice also revealed high cytotoxicity and good toleration for loaded SBA-15.[42] During investigation over 28 days, cancer growth in control and group which received pure functionalised SBA-15 were similar.[42] Two mice died from the group treated with cisplatin.[42] Mice, treated with free organotin(IV) compound, had a slower tumor grow while for immobilised into SBA-15 the tumor completely abolished.[42] Besides good cytotoxic and apoptotic activity of free (hexan-1-ol)triphenyltin(IV), drug-loaded in SBA-15 trigger additional mechanisms in tumor cells.[42] Namely, formation of melanocytes have been detected, indicating that malignant cells underwent cell differentiation. Furthermore, apoptosis of the malignant cells did not result in a typical stronger proliferation of neighboured cells.[42] The lack of changes in the group treated with pure MSNs confirms the high biocompatibility of the MSNs. *Maksimović-Ivanić et al.* studied the cellular uptake of MSNs and investigated the apoptotic effect of loaded organotin(IV) on human melanoma cells. Endocytosis of functionalised SBA-15 with particle size 650×440 nm was detected in A375 human melanoma cells.[43] The MSNs could adhere on the surface of the cells where after short treatment time, micropinocytosis could be observed.[43] Higher apoptotic and antiproliferative effects for loaded organotin(IV) compounds were observed.[43]

Although it is not completely clear, recent studies suggest that organotin(IV) immobilised into MSNs not only induce apoptosis, but may also interact with proliferative regulators and induce senescence and transdifferentiation.[42,43] This points out that such drug-vehicle combinations can be considered as high potential anticancer delivery systems with enhanced bioavailability and less toxicity.

1.7. Aim of the work

Organotin(IV) compounds provide high cytotoxic activity but their application might be limited due to their low bioavailability and toxicity. With mesoporous silica nanoparticles as drug delivery systems, bioavailability of loaded drugs can be increased while lower doses may be applied. In recent studies, organotin(IV) compounds were loaded in MSNs resulting in good or even better anticancer actions in comparison to cisplatin.

The aim of this work will be the synthesis of novel (carboxylato)organotin(IV) compounds containing nonsteroidal anti-inflammatory drugs (NSAIDs) or bioactive compounds as carboxylato ligands. That will combine both, high cytotoxicity by apoptosis (organotin(IV) moiety) and anti-inflammatory interaction in one compound. The compounds will be characterised with common methods such as ^{1}H, ^{13}C and ^{119}Sn NMR spectroscopy, electrospray ionisation mass spectrometry and elemental analysis. Due to enhanced therapeutic action for drug-loading MSNs, synthesised organotin(IV) compounds will be immobilised into MCM-41 and SBA-15. Prepared MSNs containing organotin(IV) compounds will be characterised by N_2 sorption, scanning electron microscopy, small-angle X-ray scattering and energy dispersive X-ray spectroscopy.

2. Results and discussion

2.1. Synthesis of (ferulato)triphenyltin(IV), [Ph₃Sn(fa)]

Ferulic acid was chosen as ligand due to its bioactive properties described earlier. [Ph₃Sn(fa)] was obtained in the reaction of triphenyltin(IV) chloride and ferulic acid in the presence of a base in THF at room temperature (Scheme 1).
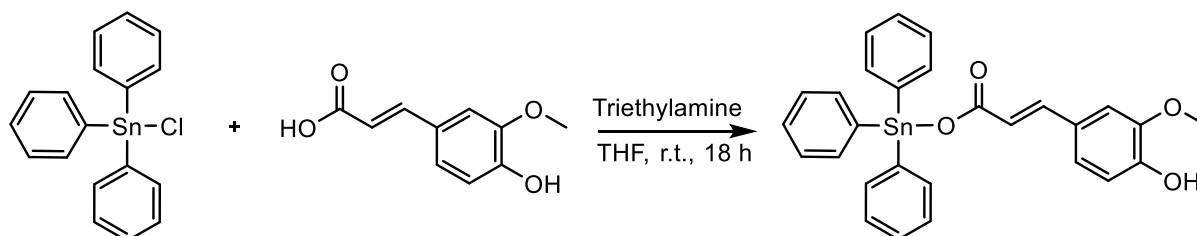
Scheme 1: Synthesis of [Ph₃Sn(fa)]

The reaction displays a nucleophilic substitution with hydrogen chloride as leaving group.[44,45] As the base takes the acidic proton, negative oxygen attacks the partially positively charged tin. During that, chloride is leaving and with triethylamine and hydrogen, triethylammonium chloride salt is formed which removes hydrogen chloride from solution. For successful synthesis of organotin(IV) compounds, usage of the base triethylamine (TEA) has been reported before and emerged.[46–49] The further advantage of the proceeding TEA hydrochloride formation is the possible precipitation as salt. Then, the purification of the desired compound should be simplified via filtration of the precipitated salt. According to that, it was important to choose a solvent which can well dissolve both precursors, but not the salt. Corresponding to *Hazardous Substances Data Bank,* the salt is not soluble in ether.[50] Based on this principle, THF was chosen as reaction solvent.

The crude product was obtained by filtration and several purification methods have been performed (recrystallisation of the salt from THF, extraction with ethyl acetate/water and DCM/water). Nevertheless, by recrystallisation, triethylammonium chloride could not be removed completely and extractions for salt removal led to decomposition of the organotin(IV) compound. As an example of purification attempts, in Figure 6 the ¹H NMR spectrum of crude [Ph₃Sn(fa)] after extraction with DCM/water is shown.
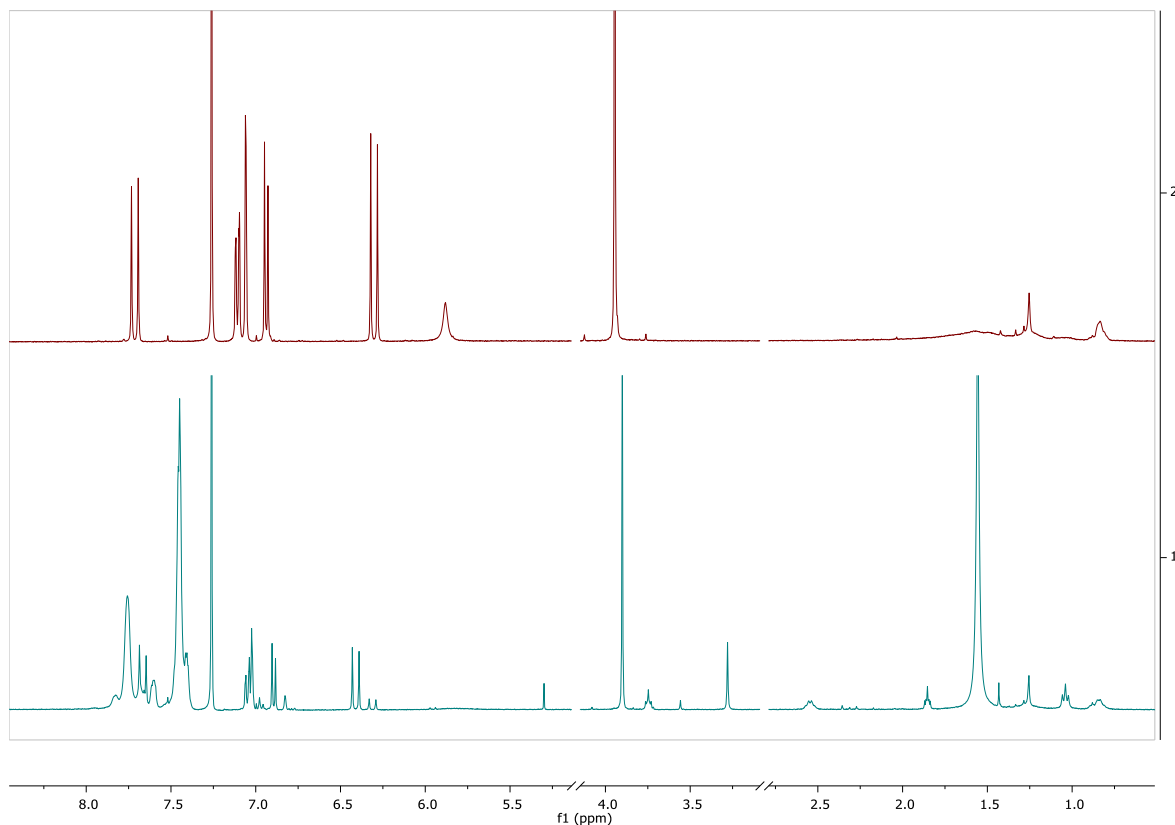
Figure 6: ^{1}H NMR spectra of fa (upper) and [Ph$_3$Sn(fa)] (lower); after extraction of the crude product with DCM/water; in CDCl$_3$.

The ^{1}H NMR analysis showed that the salt could be removed completely. Nevertheless, new chemical shifts become apparent in the neighbourhood of some hydrogen atoms from the [Ph$_3$Sn(fa)] which could not be assigned to extraction solvents, indicating a partial decomposition of the compound. ^{1}H NMR of the crude product before extraction can be seen in the appendix (Figure A 1). For both extractions, presence of distilled water was the only constant and therefore, it can be assumed that the presence of water leads to decomposition of the product. Additionally, the ligand could be involved in side reactions due to the presence of free phenolic group with a relatively high pKa of 10, which can be easily deprotonated. Nevertheless, the free carboxylic proton of pure ferulic acid could not be detected in [Ph$_3$Sn(fa)] allowing the presumption that reaction took place.

2.2. Synthesis of (4-*O*-acetylated ferulato)triphenyltin(IV), [Ph$_3$Sn(Acfa)]

As the free phenol group of the ferulic acid might be identified as a potential problem preventing the formation and purification of the desired compound, protection of this group with an acetyl function was performed. Protection of phenol group was carried out with modified literature

13

procedure.[51] Ferulic acid was protected under alkaline conditions using only 0.5 eq. of acetic anhydride. After filtration, recrystallisation and isolation under vacuum, the protected ferulic acid could be obtained. The successful protection could be confirmed with the absence of the phenolic OH proton and an acetyl group corresponding sharp resonance in ^{1}H NMR. The synthesis of [Ph$_3$Sn(Acfa)] was performed analogously to the synthesis of [Ph$_3$Sn(fa)] in THF at room temperature.
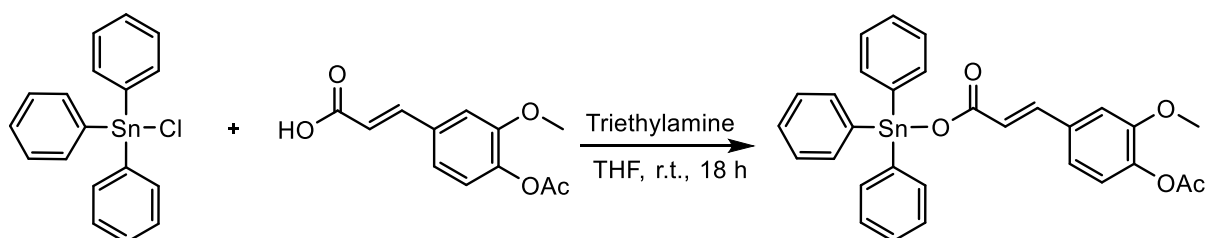
Scheme 2: Synthesis of [Ph$_3$Sn(Acfa)]

During reaction precipitated triethylammonium chloride was filtered off. Afterwards, the volume of the solvent was reduced by evaporation and stored in the freezer for several days. Upon filtration a crude product was obtained which was purified by extraction with DCM/water. The product was obtained from the organic phase as pale-yellow solid in a good yield (79%). [Ph$_3$Sn(Acfa)] was characterized with ^{1}H, ^{13}C and ^{119}Sn NMR spectroscopy, and HR-ESI-MS while purity was confirmed with elemental analysis. Triethylammonium chloride could be removed successfully via extraction. This indicates that the presence of the free phenolic group in the synthesis of [Ph$_3$Sn(fa)] most probably lead to decomposition of the compound during extraction.

The comparison between ^{1}H NMR spectroscopy of Acfa and [Ph$_3$Sn(Acfa)] can be seen in Figure 7. The complete spectra of both compounds are shown in the appendix (Figure A 2 and Figure A 3).
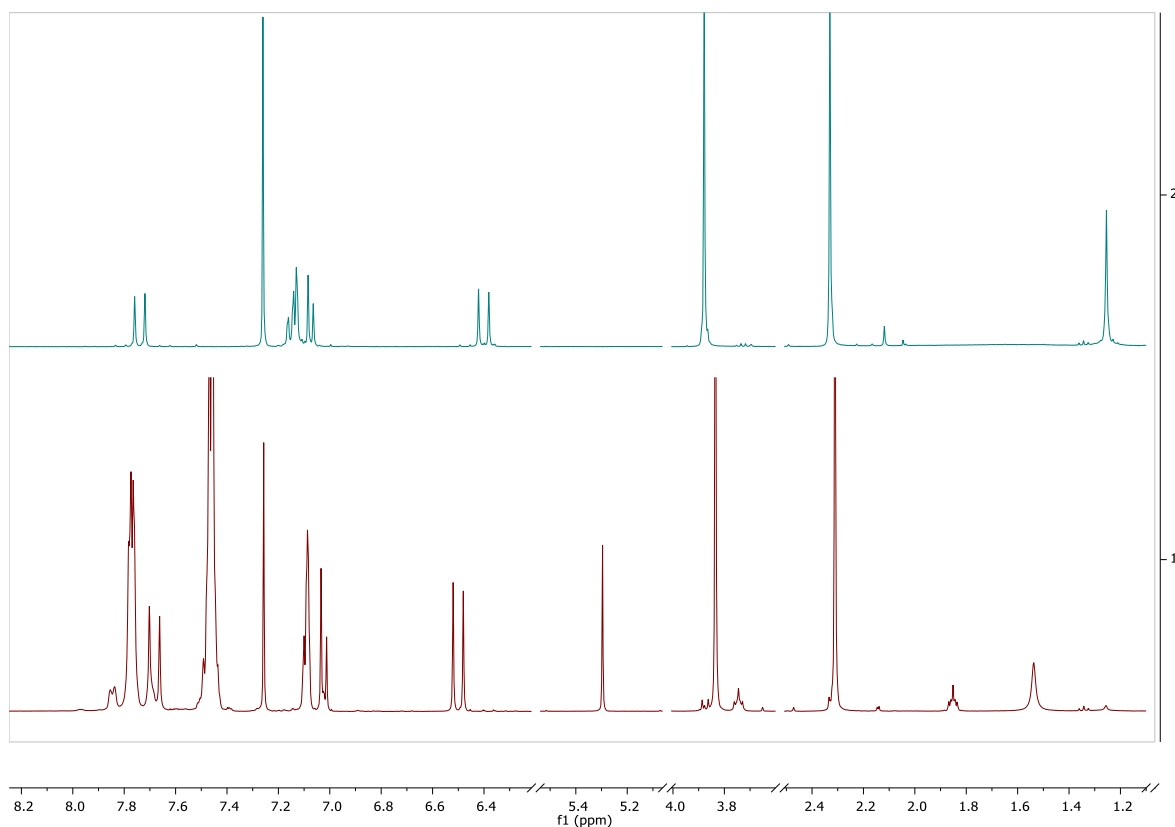
Figure 7: ^{1}H NMR spectra of Acfa (upper) and [Ph$_3$Sn(Acfa)] (lower), in CDCl$_3$

All expected resonances of the Acfa were found in [Ph$_3$Sn(Acfa)]. In the ^{1}H NMR spectrum of Acfa, the acidic H atom is not present. It is possible that acidic protons get replaced with deuterium during a proton exchange between solvent and compound.[52] All other resonances from the H atoms of protected ferulic acid shifted in the spectrum of [Ph$_3$Sn(Acfa)] especially those closer to the carboxylic group, pointing out that carboxylic group might coordinate to triphenyltin(IV) moiety. The coupling constant for vicinal protons in *trans* is higher than for *isomer* and are around 16 Hz.[52–54] In present spectrum, the doublets at 6.50 ppm and 7.68 ppm have a coupling constant $^3J_{HH}$ of 15.9 Hz each, allowing to identify them as vinylic protons of Acfa due to their neighbouring. One chemical shift from vinyl group appears more downfield in spectra of Acfa and [Ph$_3$Sn(Acfa)]. The downfield shift appears due to the induced ring current in the benzene ring of Acfa, where planar neighbours get deshielded.[52,53] Following this explanation, the resonance at 7.68 ppm can be assigned to the proton next to the benzene ring (H3', see Figure A 17). The identification of both chemical shifts from vinyl moiety were additionally confirmed with a ^{1}H,^{13}C 2D NMR spectrum. The peaks shifted for 0.6 and 0.1 ppm with higher shifts for the proton next to the carboxylic group. The sharp singlets at 2.31 and

15

3.83 ppm correspond to the methyl protons of the methoxy group and acetyl protecting group substituents at the benzene ring. The chemical shift at 3.83 ppm is caused by the more deshielded protons from the methoxy group. Therefore, the peak at 2.31 ppm can be assigned to the protons of the acetyl group. Multiplets correspond to triphenyltin(IV) moiety (at 7.47 and 7.76 ppm) provided different shifts. The multiplet of the *ortho*-protons shifted more downfield upon coordination to the tin(IV) cation, confirming an electron withdrawing neighbour next to the tin nucleus, like a carboxylic group. ^{13}C NMR spectrum of [Ph$_3$Sn(Acfa)] is shown in Figure 8.
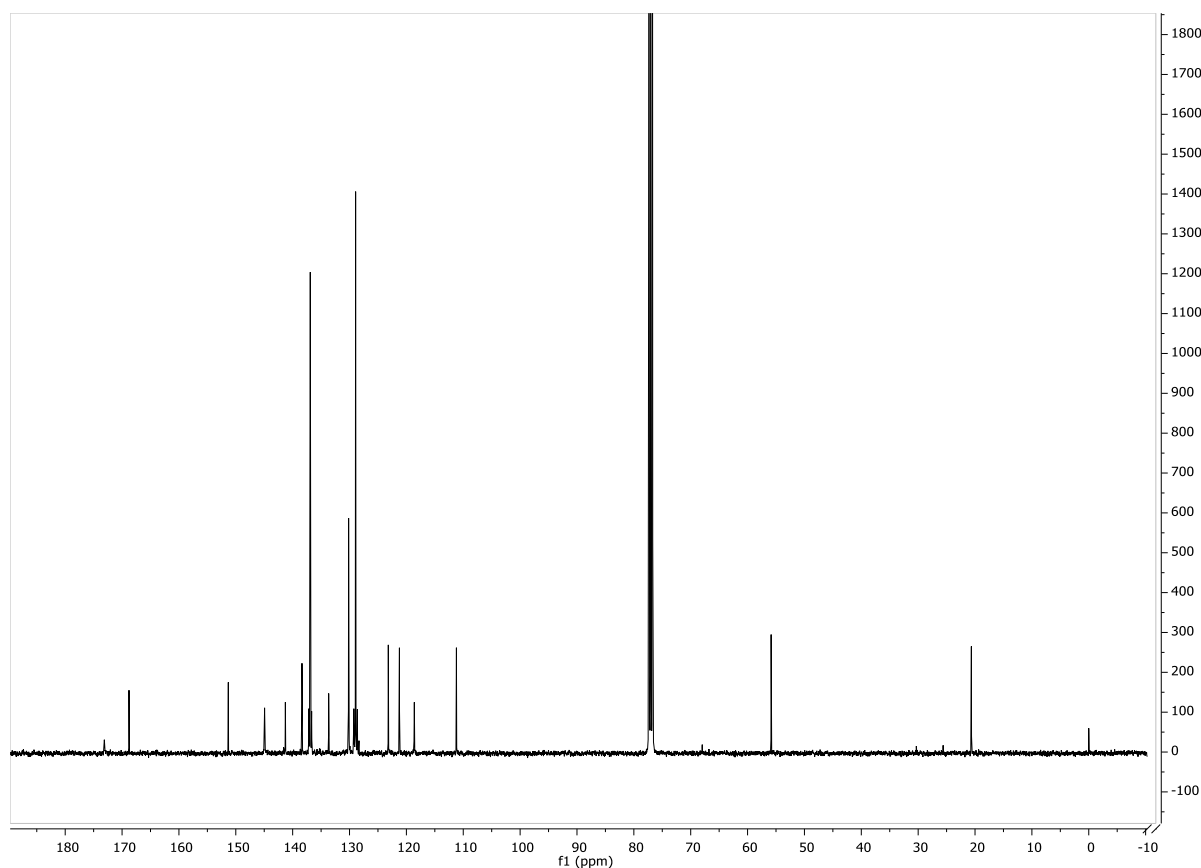
Figure 8: ^{13}C NMR spectrum of [Ph₃Sn(Acfa)], in CDCl₃

In the ^{13}C NMR spectrum of [Ph$_3$Sn(Acfa)] all carbon atom resonances from triphenyltin(IV) moiety are slightly shifted in comparison to those in Ph$_3$SnCl (i.e. *ipso* carbon atom from 137.34 to 138.36 ppm).[55] Those resonances are typical for tetrahedral coordinated tin compounds.[56] *Pellerito et al.* reported resonances of carbon atoms from ferulate anion (170.72 ppm) and as ligand (172.76 ppm).[57] The present resonance of carboxylate carbon atom is located at 173.13 ppm. Moreover, from the literature is known that vinylic carbon atoms resonances upon coordination showed shifts from 114.81 and 146.78 ppm (free fa) to 119.91 and 144.76 ppm.[57]

16

All of this confirms coordination of the carboxylate function to the tin(IV). Furthermore, 2D (^{1}H, ^{13}C) NMR spectrum facilitate signal assignment.

The ^{119}Sn NMR spectrum additionally confirmed the formation of desired compound. As it can be seen in the appendix (Figure A 4) only one chemical shift can be observed from ^{119}Sn NMR at -111.53 ppm. The resonance occurs in a typical range for tetrahedral (carboxylato)triphenyltin(IV) compounds.[42,47,56,58–60] In the HR-ESI-MS of [Ph₃Sn(Acfa)] the molecular ion peak [M+Na]$^+$ was found at 609.0685 *m/z* (see Figure A 5).

Despite the fact that several attempts for crystallisation did not lead to growth of the crystals suitable for X-ray structural analysis, the results obtained from the multinuclear NMR spectroscopy ensure that the synthesised product is the desired compound. [Ph₃Sn(Acfa)] will be used for compound-loading into MSNs.

2.3. Synthesis of (fenoprofenato)triphenyltin(IV), [Ph₃Sn(fen)]

Triphenyltin(IV) chloride was used again as starting material, due to its successful conversion previous described in 2.2. Before reaction, fenoprofen was obtained from calcium fenoprofenate dihydrate under acidic conditions. After extraction, the free fenoprofen was obtained. The synthesis of the [Ph₃Sn(fen)] was performed according modified procedure for the synthesis of [Ph₃Sn(Acfa)] using toluene as solvent, Scheme 3.
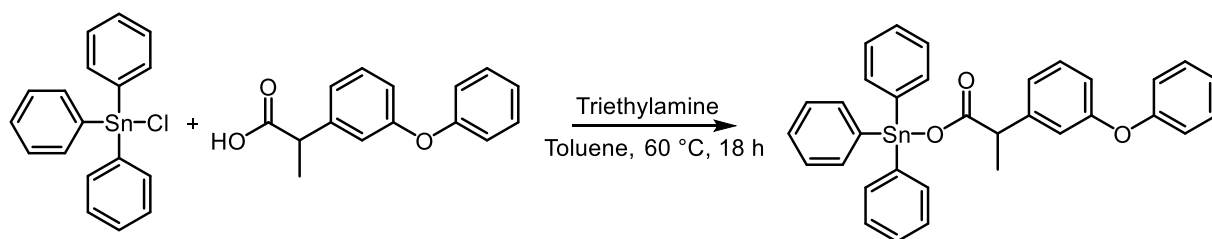
Scheme 3: Synthesis of [Ph₃Sn(fen)]

To remove precipitated salt, crude product was extracted with ethyl acetate/water leading to decomposition. Repeated recrystallisation from toluene yielded the purified compound (61.93%). [Ph₃Sn(fen)] was characterised via ^{1}H, ^{13}C and ^{119}Sn NMR spectroscopy. From the ^{1}H NMR spectrum presented in Figure 9, it came clear that toluene remained in the product. Because the immobilisation of the [Ph₃Sn(fen)] into nanoparticles takes place in toluene anyway, no further investigations were tried to remove the solvent.

17
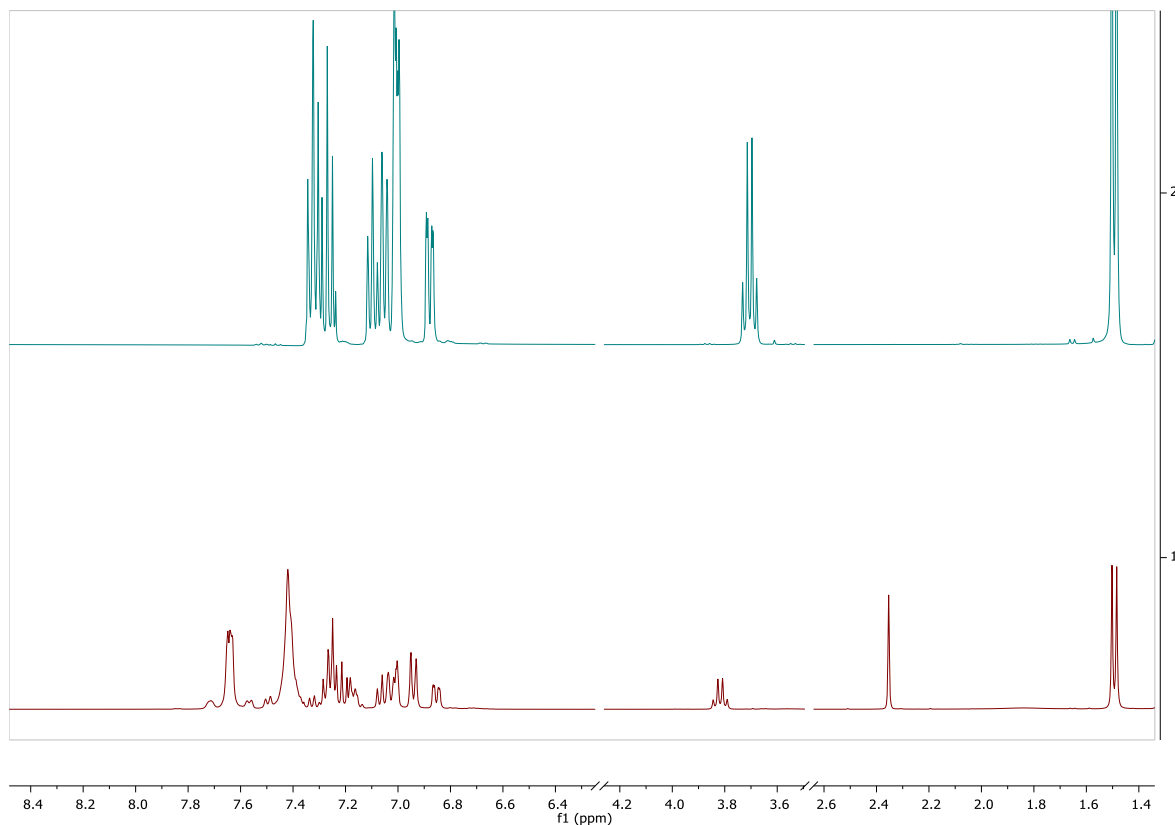
Figure 9: ^{1}H NMR spectra of fen (upper) and [Ph$_3$Sn(fen)] (lower), in CDCl$_3$

Also here, in the ^{1}H NMR spectrum a slight shift of hydrogen atom resonances from the triphenyltin(IV) moiety could be identified in comparison to [Ph$_3$SnCl]. The most prominent chemical induced shift was observed for the C*H* ($\Delta\delta$ = 3.82 ppm) from the isopropanoato moiety. The ^{13}C NMR spectrum is shown in Figure 10. Chemical shifts of the carbon atom resonances from the [Ph$_3$SnCl] were similar to those from [Ph$_3$Sn(fa)] with an *ipso* carbon atom chemical at 138.06 ppm. The resonance of the tertiary carbon atom next to the carboxylic group shifted from ppm and 18.03 to 18.97 (C2', see Figure A 18) ppm. The phenylic carbon (C1) from fen ligand shifted from 141.65 in a free acid to 143.06 ppm. Nevertheless, similar downfield shift of carbon atom resonances from the propionic acid moiety were reported for triphenyltin(IV) ibuprofen in tetrahedral coordination.[61]
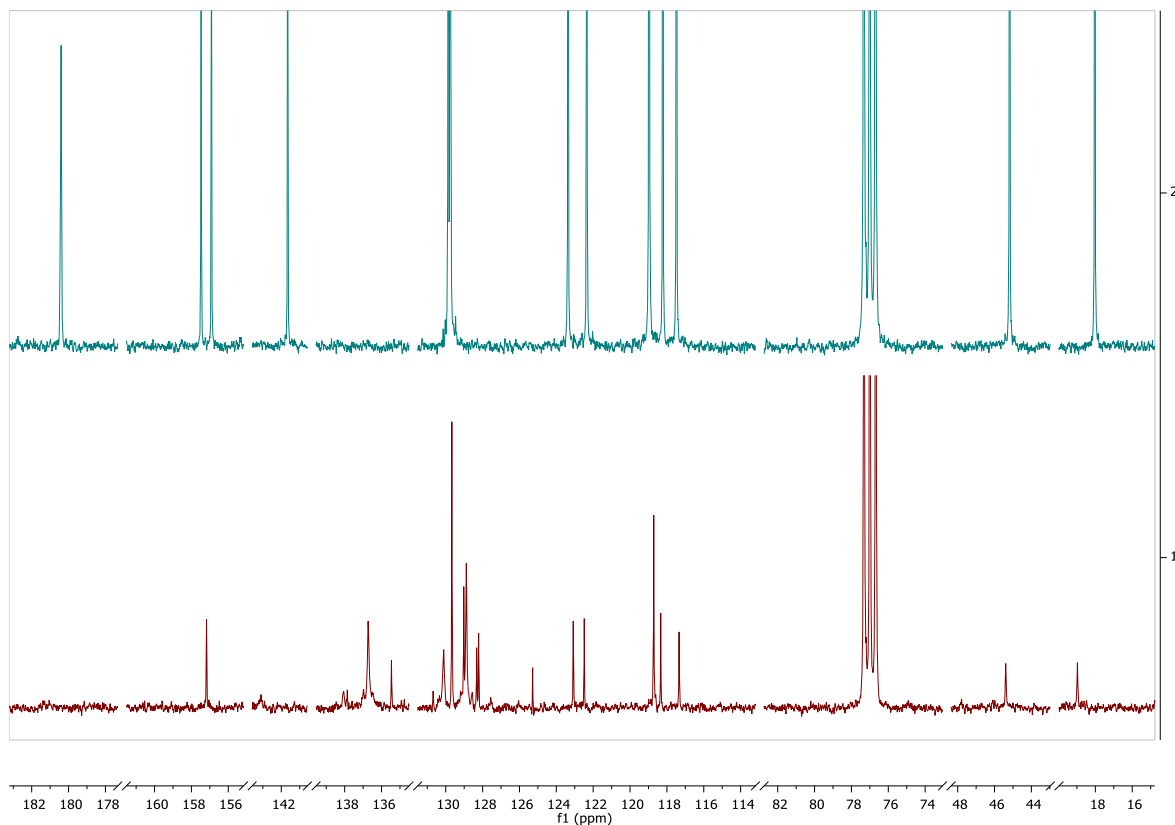
Figure 10: ^{13}C NMR spectra of fen (upper) and [Ph₃Sn(fen)] (lower), in CDCl₃

^{119}Sn NMR spectrum revealed presence of 3 different resonances, thus 3 different species. The main resonances at -107.65 ppm could be ascribed to [Ph₃Sn(fen)]. The second chemical shift in ^{119}Sn NMR spectrum at -45.39 ppm was detected and assigned to [Ph₃SnCl]. In addition, an unexpected peak at -304.08 ppm can be seen in the spectrum (Figure A 10). Peaks more upfielded than -260 ppm are from *trans*-trigonal bipyramidal penta-coordinated triphenyltin(IV) compounds.[58] The full spectra of ^{1}H and ^{13}C NMR can be seen in the appendix (Figure A 6 to Figure A 9).

In conclusion, synthesis of [Ph₃Sn(fen)] was possible, however separation did not yield pure compound.

2.4. Synthesis of (fenoprofenato)tributyltin(IV), [Bu₃Sn(fen)]

[Bu₃Sn(fen)] was prepared applying the procedure as described for [Ph₃Sn(fen)] and using [Bu₃SnCl] as starting compound. The reaction can be seen in Scheme 4.

19
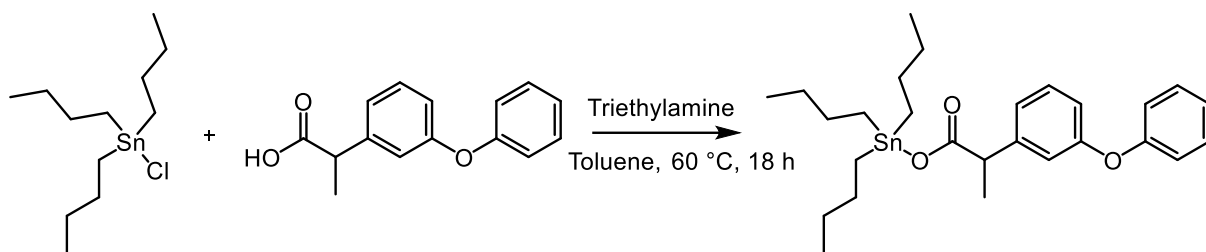
Scheme 4: Synthesis of [Bu₃Sn(fen)]

The fact that tributyltin(IV) is a liquid and fenoprofen a viscous oil becomes apparent in TEA chloride salt removal. Solvent was reduced from the reaction mixture and the pure product was obtained after full precipitation of the salt in toluene. The slightly brown sticky oil was collected after evaporation of toluene (yield of 72.1%). Figure 11 shows the ^{1}H spectra of free fenoprofen and [Bu₃Sn(fen)].
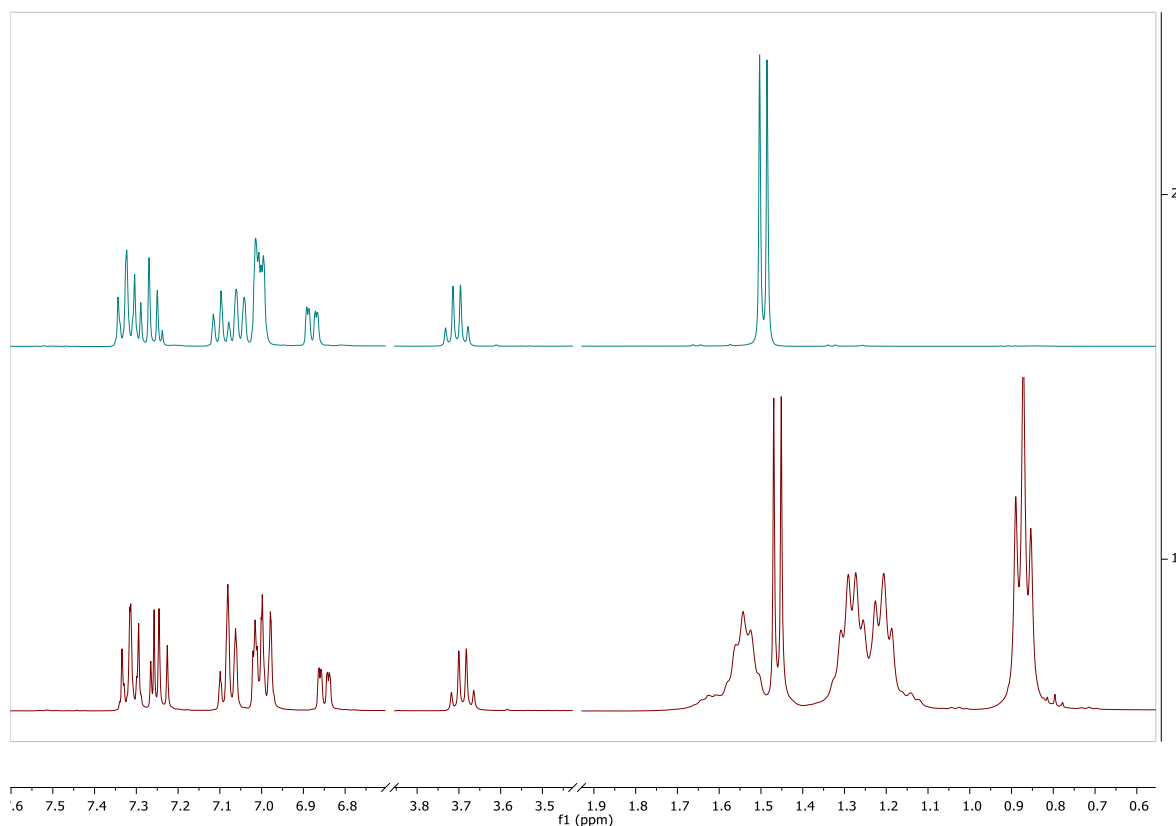
Figure 11: ^{1}H NMR spectra of fen (upper) and [Bu₃Sn(fen)] (lower), in CDCl₃

All expected protons of the synthesised product can be found in the ^{1}H NMR spectrum as well as the absence of the acidic proton from fen is evident. In pure fenoprofen resonances of

hydrogen atoms from the isopropyl group occurred at 1.49 (methyl group) and 3.71 ppm (C*H* proton from the carboxylate moiety). Both signals shifted slightly upfield to 1.46 and 3.69 ppm. Hydrogen atoms with more distance to the carboxylic group provide lower chemically induced shifts. It could be noticed that with a trialkyltin(IV) moiety the chemical induced shift becomes lower. Without electron clouds of phenyl groups around the tin, the electron density is lower and by that, the absence of an electron withdrawing effect could lead to upfield shifts. The chemical shift of methylene groups next to the tin are higher which shifted from 1.65 (tributyltin(IV) chloride) to 1.54 ppm ([Bu₃Sn(fen)]). The 9 protons at the end of the butyl groups resonated from 0.92 to 0.87 ppm. ^{13}C NMR spectrum is shown in Figure 12.
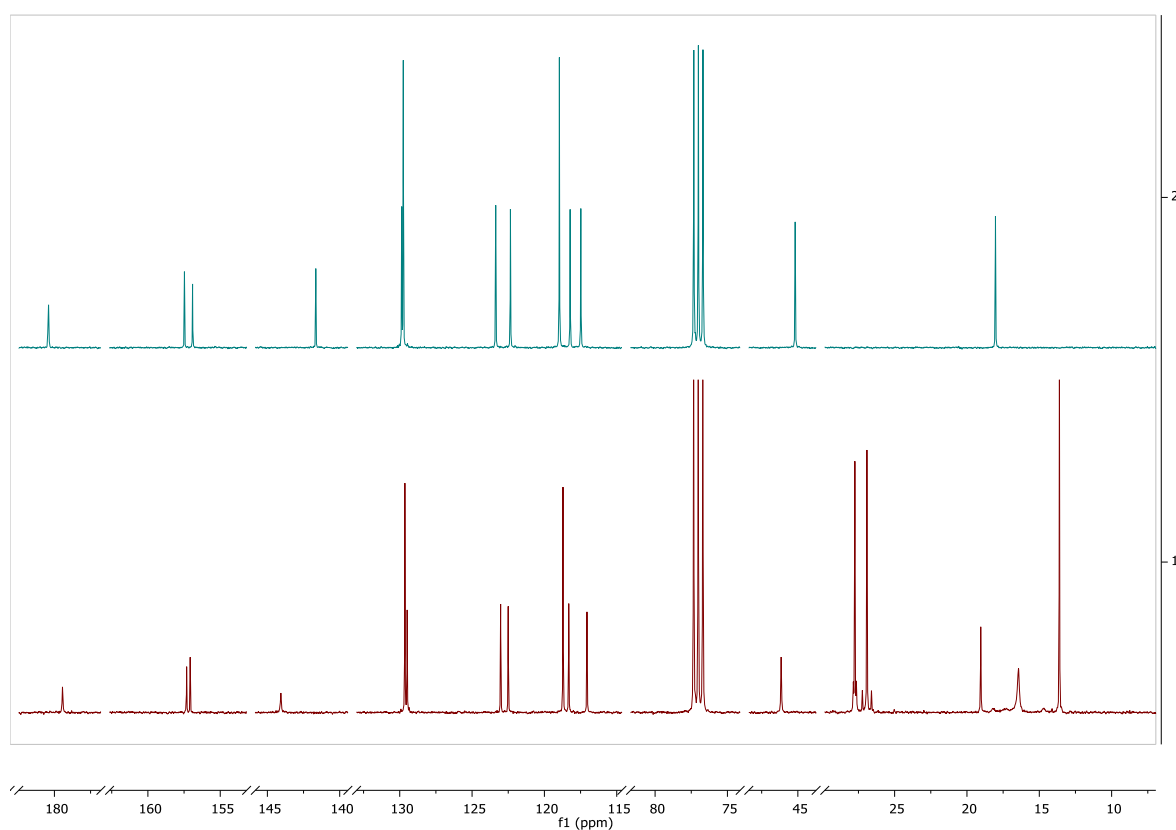
Figure 12: ^{13}C NMR spectra of fen (upper) and [Bu₃Sn(fen)] (lower), in CDCl₃

Resonances from the propionic carbon atoms shifted upon coordination up to ca 0.1 ppm. Resonances of the methyl carbon atoms (C3', see Figure A 19) and C*H* (C2') shifted from 45.19 to 46.15 ppm and 18.03 to 19.05 ppm, respectively. Thus, findings in the ^{13}C NMR spectrum suggests a coordination of the carboxylic group as well. With ^{119}Sn NMR spectroscopy there is more evidence. A resonance at 112.89 ppm for the product was observed, appearing in the frequency range for tetracoordinated tributyltin(IV) compounds.[57,61] For further

21

characterisation, HR-ESI-MS was performed, seen in Figure A 14. The peak with the highest intensity was identified as [M+Na]$^+$ with 555.1890 m/z. However, a resonance for unreacted tributyltin(IV) chloride could be detected in ^{119}Sn as well. Nevertheless, integration in ^{1}H and ^{13}C NMR spectra provides matching protons for the desired compound. Furthermore, its purification could be proofed with elemental analysis. For complete spectra see Figure A 11 to Figure A 13.

Despite the fact that several attempts for crystallisation did not lead to growth of the crystals suitable for X-ray structural analysis, the results obtained from the multinuclear NMR spectroscopy ensure that the synthesised product is the desired compound and [Bu$_3$Sn(fen)] will be used for compound-loading into MSNs.

2.5. Synthesis of MCM-41

In order to immobilise the active compounds into the two commonly used MSN, SBA-15 and MCM-41, these materials were first prepared. In fact, the SBA-15 was previously synthesised and available in the lab.[10] For the synthesis of the MCM-41 well established procedure was used.[15] Briefly, the water solution of CTAB and NaOH was heated up to 80 °C and the TEOS was added slowly. In the alkaline solution, hydrolysis of the TEOS into orthosilicic acid is catalysed and remains with negative load. The positive cationic tensides and negative silica species interact due to electrostatic interactions and the solid structure starts forming.[7,62] Filtered solid product, after calcination, yielded the solid white material.

The MCM-41 particles were characterised with a scanning electron microscope (SEM), see Figure 13.
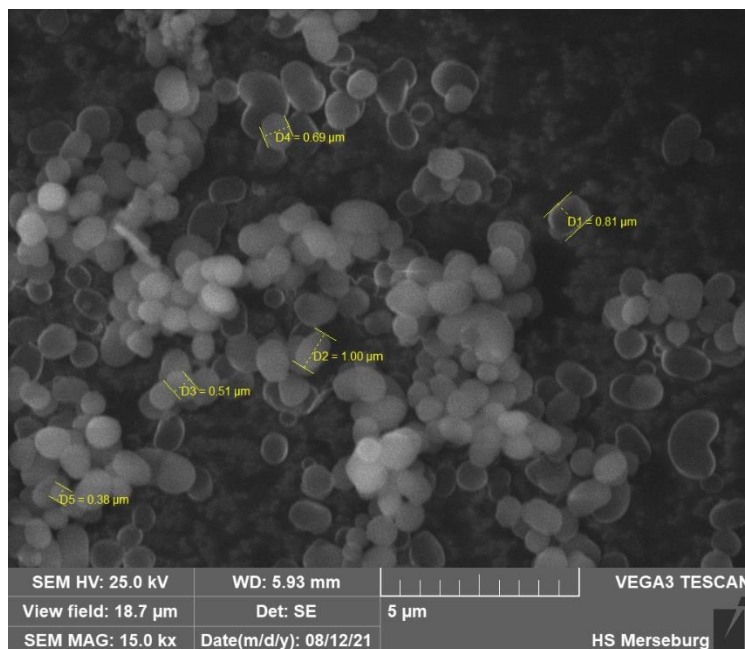
Figure 13: SEM image of MCM-41 particles, shot with 25 kV

MCM-41 particles showed spherical structures, similar to the already reported.[15,63] Several particles, however, differ in shape and agglomerated into bigger kidney-like particles. *Castillo et al.* examined conditions that can lead to coalescence of nanoparticles.[64] Temperatures above 80 °C, high CTAB/TEOS ratios and fast TEOS addition rates are identified as potential reasons. MCM-41 in present work was carried out with a CTAB/TEOS ratio of ca. 0.1, thus within recommendation range.[64] Remaining cause can be the temperature, leading to kidney-like coalescence of MCM-41 particles due to hotspots in the suspension. *Tao et al.*, whose synthesis of MCM-41 was used, reported particle sizes of around 500-900 nm.[15] Sizes for nanoparticles of MCM-41 range around 380 to 1000 nm and are less homogenous consequently. Nevertheless, they are in an expected size range.

The specific surface area of MCM-41 particles was determined with nitrogen sorption using the method of Brunauer-Emmett-Teller (BET). Nitrogen isotherms of adsorption (red) and desorption (blue) for MCM-41 are presented in Figure 14.

23
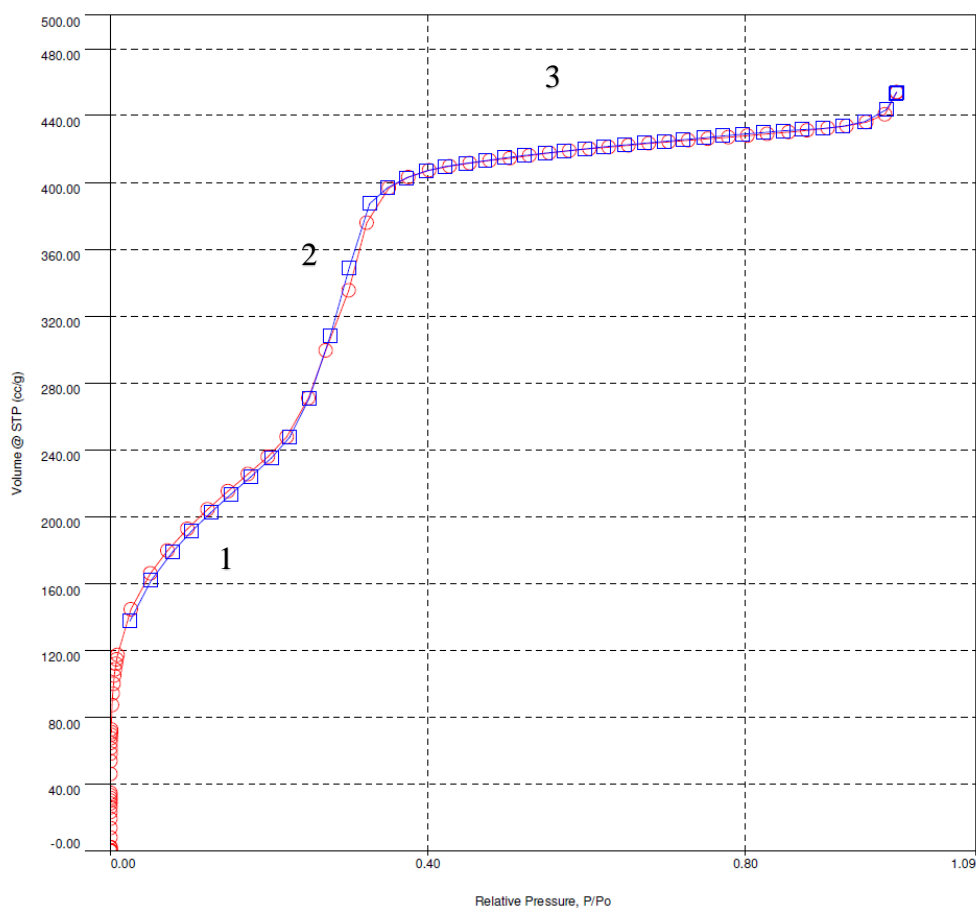
Figure 14: Adsorption and desorption isotherms of nitrogen at 77 K for MCM-41

Present adsorption and desorption isotherms correspond to isotherms type IV(a) according to IUPAC.[65] Type IV(a) corresponds to mesoporous materials and is divided into three sections.[65] The adsorption isotherm in the first section, at low pressure, increases nearly linear. With increasing pressure nitrogen constantly layers on surfaces of pore walls where each adsorbed molecule is in contact with the material, a monolayer builds up.[65] When every free place on the surface is filled, it comes to multilayer adsorption, where further molecules adsorb on the already existing monolayer.[65] The sudden rise of the isotherm marks the start of capillary condensation. Van der Waals forces in mesopores are high enough to condense the gas below its saturation vapour pressure.[65] The first section starts when pores are filled and the outer surface of each particle gets multi-layered, resulting in a plateau.[65] By comparing section 1 and 3, both linear, section 3 occurs at much higher pressures and is more extended with a smaller slope. In comparison, the range of section 1 is smaller with additionally a bigger slope. That means the mesoporous surface of present MSN is higher than the outer surface. During desorption, due to capillary condensation, forces for liquid-like gas are higher and desorption happens time-displaced, leading to a hysteresis loop.[65] For pores smaller than around 4 nm, adsorption and desorption are reversible and overlapping each other.[65] It is noticeable that there

24

is no hysteresis loop in the present BET isotherms. Filling and releasing of gas from the pores takes place at equal relative pressures. This seems to be typical for MCM-41 particles with small pores. *Schmidt et al.* have reported that when the pore size increases above 4 nm the hysteresis takes place, while below 4 nm has not been detected.[66] T-plot method revealed that no micropores are present in the MCM-41 and despite the small pore diameter, it is a mesoporous material. The multi-point BET analysis uses measured data between 0.05 and 0.3 p/p_o, providing a specific surface area of 1024 m²/g. The density functional theory (DFT) method uncovered an average pore diameter of about 2.8 nm (see Figure A 15). Barrett, Joyner, and Halenda (BJH) method led to 3.1 nm but gets more inaccurate for smaller mesopores. Both values are in a typical ranges for MCM-41 compared to literature.[15,66–69] To check the reproducibility of the isotherms, the measurement was repeated with another probe of MCM-41. As the pore diameter is smaller than 4 nm in both cases, the theory regarding the absence of hysteresis loop can be confirmed.

Comparing the properties of the MCM-41 material to the ones described by *Tao et al.,* it can be concluded that this material satisfies the requirements for a good mesoporous material and it is suitable for drug loading. With further small-angle X-ray scattering (SAXS) measurements, the lattice parameter and wall thickness can be calculated. The result of SAXS can be seen in Figure 15.
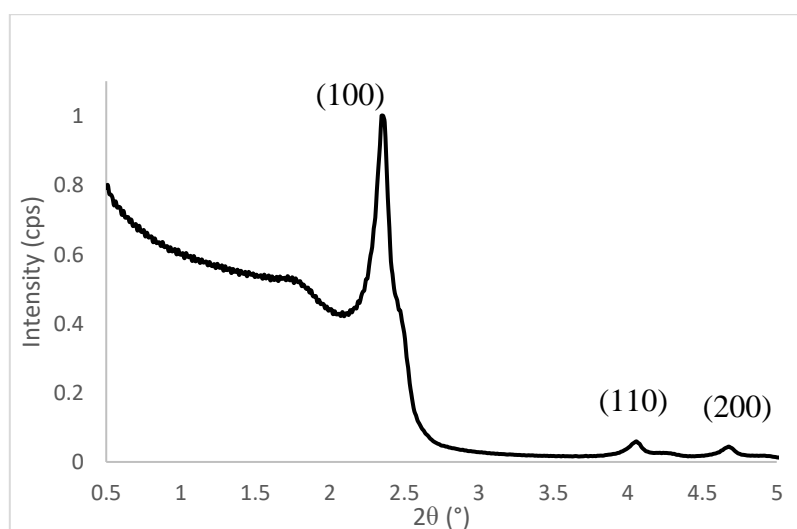

Figure 15: SAXS for MCM-41

Reflexes found in SAXS measurements provide the typical pattern for MCM-41 particles.[63,64] It proofs that pores are arranged in well-ordered hexagonal formations. Characteristic results for MCM-41 are summed up in Table 1.

Table 1: Physical properties of MCM-41

S_{BET} [m²/g]	Wall thickness [nm]	Pore diameter [nm]	Pore volume [cm³/g]	Lattice parameter [nm]	2Θ [°]	*hkl*
1024	0.96	2.8	0.63	3.76	2.3582	100
					4.0590	110
					4.6784	200

The lattice parameter of 3.76 nm was calculated from the Miller indices. In relation with pore diameter, the wall thickness can be obtained by subtracting the pore diameter from lattice parameter. Obtained values for wall thickness (0.96 nm) and a lattice parameter (3.76 nm) present typical values for MCM-41 material.[7,70,71]

2.6. Immobilised (carboxylato)triorganotin(IV) compounds into mesoporous silica nanoparticles MCM-41 and SBA-15

Nanoparticles for immobilisation were used as prepared, without further functionalisation. The mesoporous materials were first activated at 150 °C under vacuum to remove any trapped water. The two compounds [$Ph_3Sn(Acfa)$] and [$Bu_3Sn(fen)$] were loaded on both MCM-41 and SBA-15 materials, latter already synthesised by *Predarska et al*.[10] After 48 h of stirring at 80 °C, they were filtered off and the solid product was washed with toluene and *n*-pentane resulting in four drug-loaded MSNs.

To determine content of loaded organotin(IV) compounds into MSNs, EDX was performed. Results for weight% for Sn can be seen in Table 2.

Table 2: Results from EDX measurements with average values for freedraw and given errors

	freedraw		mapping	
	w% Sn	Error [%]	w% Sn	Error [%]
MCM-41|[$Ph_3Sn(Acfa)$]	16.75	12.49	16.52	5.70
MCM-41|[$Bu_3Sn(fen)$]	11.65	13.97	11.85	6.22
SBA-15|[$Ph_3Sn(Acfa)$]	17.35	15.66	16.98	5.85
SBA-15|[$Bu_3Sn(fen)$]	7.55	20.74	8.33	10.68

The table shows "freedraw" and "mapping" measurements for loaded MSNs and their accuracy as error %. Freedraw is understood to mean measurements of free chosen spots. With mapping, a greater area is measured where particle free spots are included. The homogenous distribution of Sn all over the nanoparticles could be seen using the mapping tool. Then, freedraw was used

26

to check spots in the previous area to confirm the results. As it can be seen, "freedraw" leads to higher deviations, however, detected w% of Sn are similar to values detected via mapping measurements.

A useful evaluation of compound-loading is the loading efficiency. EDX measurements only detected Si and Sn and calculated a total share of each element, given in w% without respecting other included elements, which are oxygen, hydrogen and carbon. With known molecular formula from compound and MSN it can be calculated how much share each element would have onto the whole compound-loaded MSN, resulting in a proportion between Si and Sn. This theoretical proportion can be compared with the experimental obtained one, allowing a calculated ratio between Si and Sn. For instance, the Si to Sn ratio for MCM-41|[Ph$_3$Sn(Acfa)] amounts only 94.44% of theoretically possible one, meaning only 94.44% of original used compound could be entrapped into the MSN and therefore, loading efficiency is 94.44%. Based on loading efficiency, weight% for the whole loaded compound was calculated. Loading efficiency and weight% of compound are presented in Table 3.

Table 3: Loading efficiency for organotin(IV) compounds and their share in weight% to loaded MSN

	MCM-41|[Ph$_3$Sn(Acfa)]	MCM-41|[Bu$_3$Sn(fen)]	SBA-15|[Ph$_3$Sn(Acfa)]	SBA-15|[Bu$_3$Sn(fen)]
Loading efficiency [%]	94.44	58.17	89.81	35.73
w% of compound in material	35.19	24.59	34.01	17.55

Lower loading for [Bu$_3$Sn(fen)] in respect to [Ph$_3$Sn(Acfa)] comes apparent from loading efficiency. Lesser loading of [Bu$_3$Sn(fen)] into MSNs can be explained by the good solubility of this compound in toluene and therefore, a smaller driving force for its absorption into mesopores of MSN. Furthermore, washing procedure was carried out with toluene and *n*-pentane. Due to solubility, MSN|[Bu$_3$Sn(fen)] was washed only with 20 mL of toluene, however this process could remove the entrapped compound as well. Nevertheless, 17.55 w% of compound still provide high loading.[11,42,43]

It is important that upon immobilisation of the compounds into MSNs the mesoporous materials keep their structure and no change of particle size or shape occurs. To examine this, for all loaded MSNs SEM analysis was performed. Resulting SEM images of all compound-loaded MSNs can be seen in Figure 16.
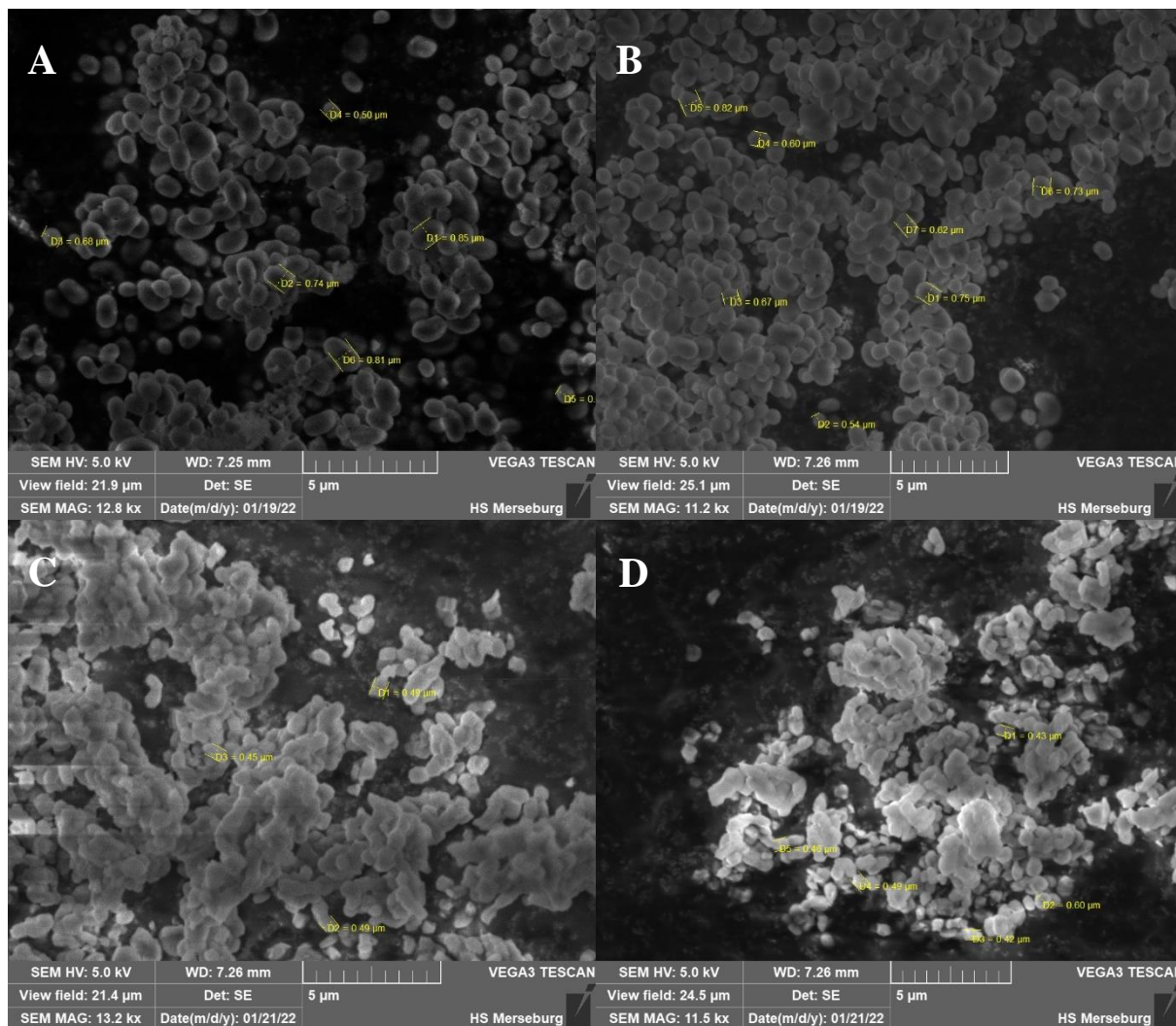
Figure 16: SEM images of MCM-41|[Ph₃Sn(Acfa)] (A), MCM-41|[Bu₃Sn(fen)] (B), SBA-15|[Ph₃Sn(Acfa)] (C) and SBA-15|[Bu₃Sn(fen)] (D)

From the obtained results, it can be seen that the compound-loading did not cause any damage of the mesoporous material. The size as well as the spherical shape of MCM-41 particles and rod-shape of SBA-15 particles could be retained.

The results of SAXS measurements of pure and compound-loaded MSNs are presented in Figure A 16 in the appendix. Patterns for the materials SBA-15 and MCM-41 are different, due to reflexes at different angles. Nevertheless, both materials provide same patterns for without and with compound, therefore hexagonal pore arrangement has not changed. Resulting wall thickness for SBA-15|[Ph₃Sn(Acfa)] is 5.2 nm. In respect of pure SBA-15 from *Predarska et al.* wall thickness, 3.66 nm, increased upon loading, as expected.[10]

To investigate how the loading of organotin(IV) compound influenced the specific surface area N_2 adsorption and desorption isotherms were measured. For MSNs a multi-point BET analysis was performed, where the adsorption isotherms are detected to determine the specific surface area. Additionally for SBA-15|[Ph₃Sn(Acfa)] the pores size and volume of the mesoporous material was measured.

As expected, Figure 17 shows type IV isotherms with type I hysteresis loop characteristic for SBA-15 material.[10,65]
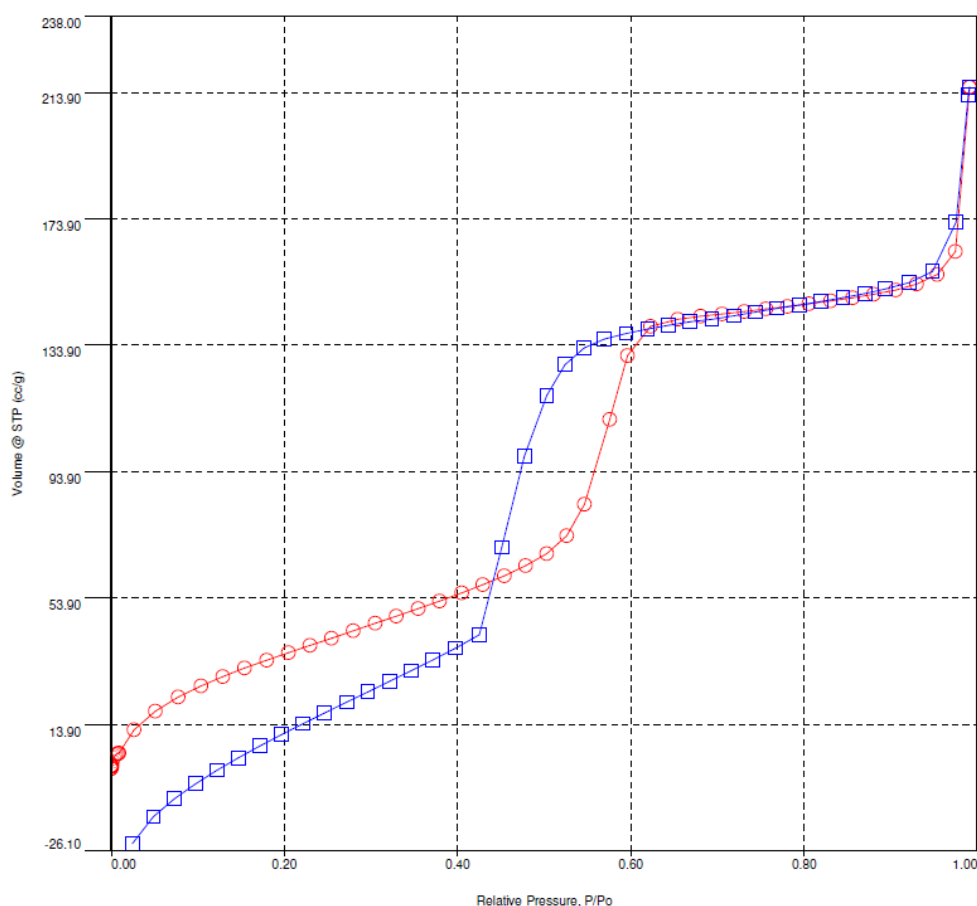
Figure 17: Adsorption and desorption isotherms of nitrogen at 77 K for SBA-15|[Ph₃Sn(Acfa)]

Hysteresis loop type I indicates capillary condensation for pore diameters larger than 4 nm. Present desorption isotherm sinks below adsorption curve indicating that more was desorbed than adsorbed, resulting from finished outgassing, before experiment was complete. Important are pore volume and specific surface area. BJH method reveals pore volume of 0.44 cm³/g and the probe provides a specific surface area (BET) of 158 m²/g. In comparison, values for pure SBA-15 were 0.72 cm³/g and 517 m²/g respectively. Because [Ph₃Sn(Acfa)] is immobilised in the pores of SBA-15, it is expected that free pore volume is decreased. Therefore, the BET measurement confirms successful loading of the compound into SBA-15.

The specific surface area of SBA-15|[Bu$_3$Sn(fen)] is found to be 336 m²/g, thus larger than for [Ph$_3$Sn(Acfa)]. Indeed, less loaded compound results in a less decreased surface area and confirms lower load extent for SBA-15|[Bu$_3$Sn(fen)]. Specific surface areas of MCM-41|[Ph$_3$Sn(Acfa)] and MCM-41|[Bu$_3$Sn(fen)] are 776 m²/g and 887 m²/g respectively. Without desorption isotherm it is not possible to calculate the pore volume but decreased BET surface areas suggest successful compound loading as well.

All used characterisation techniques (EDX, BET, SEM and SAXS) confirmed loading of (carboxylate)triorganotin(IV) compounds into MSNs with success and without physical changes of the material.

3. Conclusion

Organotin(IV) compounds are potentially outstanding candidates for cancer therapy as they provide very high cytotoxicity. Nevertheless, they are associated with many side effects as well and therefore, up to now they have not been used in clinical therapy. Their limited solubility in water leads to low bioavailability and the need for high doses to be applied in order to achieve desired therapeutic effects is necessary. With evidence that inflammation is related to the development and progression of cancer, anti-inflammatory drugs and antioxidant agents with similar effects gain interest. Usage of NSAIDs drugs as ligands bonded to metal centers, both anti-inflammatory drug and cytotoxic active agent can be conjugated in one compound with dual action in the treatment of cancer cells.

Mesoporous silica nanoparticles provide a promising strategy for drug delivery application. These nanoparticles with large surface area show high biocompatibility *in vivo.* Furthermore, their low-cost synthesis under moderate conditions as well as the highly adjustable properties, like size and shape, make them good drug delivery vehicles. Loading metal-based drugs into MSNs can be beneficial for overcoming problems with drugs' solubility and *in vivo* stability and finally lead to better bioavailability.

Two organotin(IV) carboxylates were successfully synthesised and characterised during this work. Namely, one triphenyltin(IV) compound, [$Ph_3Sn(Acfa)$], and one tributyltin(IV) compound, [$Bu_3Sn(fen)$], with high yields (72–79%).

Prepared (carboxylato)organotin(IV) compounds, [$Ph_3Sn(Acfa)$] and [$Bu_3Sn(fen)$], were immobilised into two mesoporous silica materials, MCM-41 and SBA-15. Tin content in MSNs was found from 7.55–16.75%, with a loading efficiency of 35.73–94.44%. Upon immobilisation of organotin(IV) compounds nanomaterials retained shape and morphology.

The biological activity of these compounds and materials needs to be further investigated with *in vitro* cytotoxicity studies on cancer cells.

4. Experimental part

4.1. Materials and methods

All reactions were performed under nitrogen atmosphere using standard Schlenk technique. Reagents, except fenoprofen and protected ferulic acid, were commercially available and used as purchased: triphenyltin(IV) chloride (Alfa Aesar, 95%), *trans*-ferulic acid (99%), tetraethyl orthosilicate (Sigma), fenoprofen calcium dihydrate (TRC), tributyltin(IV) chloride (Acros Organics, 95%), cetyltrimethylammonium bromide (abcr). Triethylamine, tetrahydrofuran and toluene were used dry.

4.1.1. Characterisation of organotin(IV) compounds

Synthesised compounds were characterised with multinuclear NMR Spectroscopy on a Bruker AVANCE DRX 400 spectrometer and measured in $CDCl_3$. Spectra ^{1}H (400.131 MHz), ^{13}C (100.63 MHz) and ^{119}Sn (149.2 MHz) are referenced to tetramethylsilane as internal standard. HR-ESI mass spectra were recorded with a Bruker Daltonics mass spectrometer.

4.1.2. Characterisation of mesoporous silica nanoparticles

Scanning electron microscopy and energy dispersive X-ray imaging were performed on a TESCAN VEGA$_3$ microscope with an element detector from EDAX Inc. Brunauer-Emmet-Teller physisorption and probe outgassing (350 °C pure MSN, 130 °C loaded MSN) were performed on Autosorb iQ/ASiQwin from Quantochrome Instruments. Small Angle X-ray Scattering was performed on a D8 ADVANCE from Bruker.

4.2. Synthesis of SBA-15

SBA-15 was synthesised from *Predarska et al.* with literature reported procedure.[10] Briefly, P123 (48.4 g) was dissolved at 35 °C in H_2O (360 mL) and HCl (2 M, 1400 mL). Next, TEOS (102 g) was added dropwise and the reaction mixture was vigorously stirred at 35 °C for 20 h and for additional 24 h at 80 °C. Upon filtration and drying (14 h at 90 °C), the obtained material was calcified by heating (1 °C min$_{-1}$) to 500 °C and holding at this temperature for 24 h.

4.3. Synthesis of MCM-41

MCM-41 was synthesised according to literature.[15] First, 11.0 mmol (4 g) CTAB were dissolved with 960 mL distilled water (dH_2O) and 14 mL 2.0 M NaOH. The solution was stirred for 30 min at 80 °C. Then, 101.2 mmol (21.0 g) TEOS were added dropwise into the reaction solution, afterwards stirred for 2 h at 80 °C. The product was filtered while still hot and the

solid was washed with copious amounts of dH$_2$O and ethanol. The resulting precipitate was dried overnight at 80 °C. To remove the surfactant template from the material, the MCM-41 was calcified at 550 °C for 5 h with a heating rate of 1 °C per minute.

Yield: 2.29 g (75.67%)

Specific surface area (BET): 1024 m²/g

Pore volume (DFT): 0.63 cm³/g

Pore diameter (DFT): 2.8 nm

4.4. Protected ferulic acid

Ferulic acid was protected with an acetyl group following slightly modified literature procedure.[51] 1 g of ferulic acid were dissolved in 15 mL 1M NaOH while stirring. 1 mL of acetic anhydride was added and the solution was stirred for 2 hours in an ice bath. The product was isolated using vacuum filtration through a Büchner funnel, washed with ice-cold distilled water and recrystallized from 15 mL of boiling ethanol to afford the pure product as white solid.

¹H NMR (400 MHz, CDCl$_3$, ppm): 7.74 (d, $^3J_{HH}$ = 16.0 Hz, 1H, CH$_{vin}$), 7.14 (td, 2H, CH$_{aromat}$), 7.07 (d, $^3J_{HH}$ = 8.1 Hz, 1H, CH$_{aromat}$), 6.40 (d, $^3J_{HH}$ = 15.9 Hz, 1H, CH$_{vin}$), 3.88 (s, 3H, OCH$_3$), 2.33 (s, 3H, OCOCH$_3$)

4.5. Preparation of fenoprofen

Fenoprofen is commercially available as dihydrate calcium salt. To obtain the monocarboxylic free acid, 2 g of fenoprofen calcium salt were dissolved in 60 mL of 2 M hydrochloric acid. The solution was stirred overnight at 60 °C. The product was extracted with ethyl acetate and distilled water. The organic phase was collected and dried on rotational evaporator to obtain the product as a colourless oil.

¹H NMR (400 MHz, CDCl$_3$, ppm): 7.37 – 7.28 (m, 2H, CH$_{aromat}$), 7.31 – 7.22 (m, 1H, CH$_{aromat}$), 7.14 – 7.02 (m, 2H, CH$_{aromat}$), 7.02 – 6.99 (m, 2H, CH$_{aromat}$), 6.88 (dd, $^3J_{HH}$ = 8.2, 2.0 Hz, 1H, CH$_{aromat}$), 3.71 (q, $^3J_{HH}$ = 7.2 Hz, 1H), 1.49 (d, $^3J_{HH}$ = 7.2 Hz, 3H, CH$_{aliphat}$)

4.6. Synthesis of organotin(IV) compounds

4.6.1. (Ferulato)triphenyltin(IV), [Ph$_3$Sn(fa)]

0.4 g of triphenyltin(IV) chloride (1.04 mmol) and 0.202 g (1.04 mmol) of ferulic acid were weighed, consecutively, in Schlenk flask. Dry tetrahydrofuran (30 mL) was added and the

solution was stirred for 15 min at room temperature. After addition of triethylamine 0.29 mL (2.08 mmol).) to the reaction mixture, stirring was continued overnight at room temperature. The formed precipitate of triethylammonium chloride salt was separated by filtration and the solvent was removed under reduced pressure. Recrystallisation attempts were carried out in THF in the freezer. Extraction took place in a separator with ethyl acetate/water and DCM/water, leading to decomposition.

^{1}H NMR (400MHz, CDCl$_3$, ppm): 7.80 – 7.74 (m, 6H, CH_{aromat}), 7.64 (d, $^3J_{HH}$ = 15.8 Hz, 1H, CH_{vin}), 7.48 – 7.42 (m, 9H, CH_{aromat}), 7.07 – 7.01 (m, 2H, CH_{aromat}), 6.89 (d, $^3J_{HH}$ = 8.0 Hz, 1H, CH_{aromat}), 6.41 (d, $^3J_{HH}$ = 15.8 Hz, 1H, CH_{vin}), 3.89 (s, 3H, OCH_3)

4.6.2. (4-*O*-acetylated ferulato)triphenyltin(IV), [Ph$_3$Sn(Acfa)]

For the preparation of [Ph$_3$Sn(Acfa)] procedure described in 4.6.1. was used, with 0.245 g (1.04 mmol) of 4-*O*-acetylated ferulic acid instead of ferulic acid. To obtain a pure product, DCM/water extraction was carried out. Afterwards, [Ph$_3$Sn(Acfa)] was obtained by solvent removal from the organic phase as pale yellow solid. For numeration of H and C atoms see Figure A 17.

Yield: 0.48 g (79.0%)

^{1}H NMR (400 MHz, CDCl$_3$, ppm): 7.81 – 7.74 (m, 6CH, Hb), 7.68 (d, $^3J_{HH}$ = 15.9 Hz, 1CH, H3'), 7.52 – 7.41 (m, 9CH, Hc, Hd), 7.11 – 7.07 (m, 2CH, H5, H6), 7.02 (d, $^3J_{HH}$ = 8.6 Hz, 1CH, H2), 6.50 (d, $^3J_{HH}$ = 15.9 Hz, 1CH, H2'), 3.83 (s, OCH_3, H4'), 2.31 (s, OCOCH_3, H6'),

^{13}C{^{1}H} NMR (100 MHz, CDCl$_3$, ppm): 173.12 (*C*OO, C1'), 168.78 (O*C*OCH$_3$, C5'), 151.31 (*C*OAc, C4), 144.94 (*C*H, C3′), 141.28 (*C*OCH$_3$, C3), 138.36 (3*C*Sn, Ca), 136.9 (6*C*H, Cb), 133.67 (*C*, C1), 130.16 (3*C*H, Cd), 128.93 (6*C*H, Cc), 123.18 (*C*H, C2), 121.23 (*C*H, C5), 118.60 (*C*H, C2'), 111.20 (*C*H, C6), 55.86 (O*C*H$_3$, C4'), 20.64 (OCO*C*H$_3$, 6')

^{119}Sn{^{1}H} NMR (149 MHz, CDCl$_3$, ppm): δ –111.53

Elemental analysis: calculated (%) for C$_{30}$H$_{26}$O$_5$Sn: C 61.6, H 4.5; found: 61.38, H 4.41.

HR-ESI-MS (positive mode): *m/z* [M-Na]$^+$: calculated for C$_{30}$H$_{26}$O$_5$Sn: 609.0694, found: 609.0685

4.6.3. (Fenoprofenato)triphenyltin(IV), [Ph$_3$Sn(fen)]

Triphenyltin(IV) chloride 0.4 g (1.04 mmol) and fenoprofen 0.25 g (1.04 mmol) were weighed, consecutively, in Schlenk flask. Dry toluene (30 mL) was added and the solution was stirred

for 15 min at 60 °C. After addition of triethylamine 0.29 mL (2.08 mmol) to the reaction mixture, stirring was continued overnight at 60 °C. The formed precipitate of triethylammonium chloride salt was separated by filtration and the solvent was removed under reduced pressure yielding crude product as white sticky solid. All attempts of purification (recrystallization from toluene and extraction with ethyl acetate/water) could not yield pure [Ph$_3$Sn(fen)]. The impurity was identified as [Ph$_3$SnCl] starting compound. For numeration of H and C atoms see Figure A 18.

Yield: 0.38 g (61.93 %)

^{1}H NMR (400 MHz, CDCl$_3$, ppm): 7.74 – 7.54 (m, 6C*H*, Hb), 7.52 – 7.31 (m, 9C*H*, Hc, Hd), 7.30 – 7.15 (m, 3C*H*, H3, H9, H11), 7.09 – 7.03 (m, 2C*H*, H2, H10), 7.02 – 6.98 (m, 2C*H*, H8, H12), 6.85 (dd, $^3J_{HH}$ = 8.2, 1.5 Hz, 1C*H*, H4), 3.82 (q, $^3J_{HH}$ = 7.1 Hz, C*H*, H2'), 1.49 (d, $^3J_{HH}$ = 7.1 Hz, C*H*$_3$, H3'), H6 not detectable

^{13}C{^{1}H} NMR (100 MHz, CDCl$_3$, ppm): 157.18 (2*C*O, C5, C7), 143.06 (*C*, C1), 136.72 (3*C*Sn, Ca), 135.46 (6*C*H, Cb), 130.12 (3*C*H, Cd), 129.67 (2*C*H, C9, C11), 129.02 (*C*H, C3), 128.88 (6*C*H, Cc), 123.08 (*C*H, C2), 122.48 (CH, C10), 118.71 (2*C*H, C8, C12), 118.33 (*C*H, C6), 117.34 (*C*H, C4), 45.39 (*C*H, C2'), 18.97 (*C*H$_3$, C3'), C1' not detectable

^{119}Sn{^{1}H} NMR (149 MHz, CDCl$_3$, ppm): δ –45.40, –107.84

Elemental analysis: calculated (%) for C$_{33}$H$_{28}$O$_3$Sn: C 67.03, H 4.77; found: C 64.89, H 4.60

HR-ESI-MS (positive mode): *m/z* [M-Na]$^+$: calculated for C$_{33}$H$_{28}$O$_3$Sn: 615.0952, found: 615.0992

4.6.4. (Fenoprofenato)tributyltin(IV), [Bu$_3$Sn(fen)]

For the preparation of [Bu$_3$Sn(fen)] procedure described in 4.6.3 was used, using 0.34 g of tributyltin(IV) chloride (1.04 mmol) instead of triphenyltin(IV) chloride. The formed precipitate of triethylammonium chloride salt was separated by filtration and the solvent was removed under reduced pressure to obtain the product as brown sticky oil. For numeration of H and C atoms see Figure A 19.

Yield: 0.40 g (72.07 %)

^{1}H NMR (400 MHz, CDCl$_3$, ppm): 7.37 – 7.28 (m, 2C*H*, H9, H11), 7.27 – 7.22 (m, 1C*H*, H3), 7.12 – 7.05 (m, 2C*H*, H2, H10), 7.04 – 6.95 (m, 2C*H*, H8, H12), 6.85 (dd, $^3J_{HH}$ = 8.1, 1.6 Hz, 1C*H*, H4), 3.69 (q, $^3J_{HH}$ = 7.1 Hz, C*H*, H2'), 1.55 (p, $^3J_{HH}$ = 7.7 Hz, 3C*H*$_2$, Ha), 1.46 (d, $^3J_{HH}$ =

7.1 Hz, C*H*$_3$, H3'), 1.29 (q, $^3J_{HH}$ = 7.4 Hz, C*H*$_2$, Hc), 1.26 – 1.17 (m, C*H*$_2$, Hb), 0.87 (t, $^3J_{HH}$ = 7.3 Hz, 3C*H*$_3$, Cd), H6 not detectable

^{13}C{^{1}H} NMR (100 MHz, CDCl$_3$, ppm): 179.44 (*C*OO, C1'), 157.32 (*C*O, C5), 157.08 (*C*O, C7), 144.07 (*C*, C1), 129.64 (2*C*H, C9, C11), 129.49 (*C*H, C3), 123.03 (*C*H, C2), 122.50 (CH, C10), 118.71 (2*C*H, C8, C12), 118.32 (*C*H, C6), 117.06 (*C*H, C4), 46.15 (*C*H, C2'), 27.75 (3*C*H$_2$, Ca), 26.92 (3*C*H$_2$, Cc), 19.05 (*C*H$_3$, C3'), 16.44 (3*C*H$_2$, Cb), 13.61 (3*C*H$_3$, Cd)

^{119}Sn{^{1}H} NMR (149 MHz, CDCl$_3$, ppm): δ 112.89

Elemental analysis: calculated (%) for C$_{27}$H$_{40}$O$_3$Sn: C 61.04, H 7.59; found: C 60.51, H 7.55

ESI-MS (positive mode): *m/z* [M-Na]$^+$: calculated for C$_{27}$H$_{40}$O$_3$Sn: 555.1891, found: 555.1890

4.7. Preparation of drug-loaded nanoparticles

The immobilisation of organotin(IV) compounds into MSNs followed the procedure, similar to one reported in literature.[43] The organotin(IV) compounds were suspended or dissolved in toluene and added to the MSN material previously activated by drying under vacuum at 150 °C for 16 h. The reaction mixture was stirred at 80 °C for 48 h. The obtained material was isolated by filtration followed by successive washing with toluene and n-pentane. The obtained drug-loaded MSNs were dried at room temperature.

MCM-41|[Ph$_3$Sn(Acfa)]: 100 mg of [Ph$_3$Sn(Acfa)], 220 mg of MCM-41a; yield: 268.4 mg, BET surface: 777 m²/g, SAXS (2θ in °, Miller indices): 2.3582 (100), 4.059 (110), 4.6784 (200)

MCM-41|[Bu$_3$Sn(fen)]: 100 mg of [Bu$_3$Sn(fen)], 220 mg of MCM-41a; yield: 236.5, BET surface: 887 m²/g, SAXS (2θ in °, Miller indices): 2.3687 (100), 4.059 (110), 4.6784 (200)

SBA-15|[Ph$_3$Sn(Acfa)]: 100 mg of [Ph$_3$Sn(Acfa)], 200 mg of SBA-15; yield: 264.1 mg, BET surface: 158 m²/g, SAXS (2θ in °, Miller indices): 1.0354 (100), 1.7178 (110), 2.0328 (200)

SBA-15|[Bu$_3$Sn(fen)]: 100 mg of [Bu$_3$Sn(fen)], 200 mg of SBA-15; yield: 203.6 mg, BET surface: 336 m²/g, SAXS (2θ in °, Miller indices): 1.0459 (100), 1.7493 (110), 2.0328 (200)

5. References

1. Rosenberg B, van Camp L, Krigas T. Inhibition of Cell Division in Escherichia coli by Electrolysis Products from a Platinum Electrode. *Nature.* 1965;205:698–699.

2. Anthony EJ, Bolitho EM, Bridgewater HE, Carter OWL, Donnelly JM, Imberti C, Lant EC, Lermyte F, Needham RJ, Palau M, Sadler PJ, Shi H, Wang F-X, Zhang W-Y, Zhang Z. Metallodrugs are unique: opportunities and challenges of discovery and development. *Chemical Science.* 2020;11(48):12888–12917.

3. Bulatović MZ, Maksimović-Ivanić D, Bensing C, Gómez-Ruiz S, Steinborn D, Schmidt H, Mojić M, Korać A, Golić I, Pérez-Quintanilla D, Momčilović M, Mijatović S, Kaluđerović GN. Organotin(IV)-loaded mesoporous silica as a biocompatible strategy in cancer treatment. *Angewandte Chemie International ed.* 2014;53(23):5982–5987.

4. Barabas K, Milner R, Lurie D, Adin C. Cisplatin: a review of toxicities and therapeutic applications. *Veterinary and Comparative Oncology.* 2008;6(1):1–18.

5. Banti CN, Hadjikakou SK, Sismanoglu T, Hadjiliadis N. Anti-proliferative and antitumor activity of organotin(IV) compounds. An overview of the last decade and future perspectives. *Journal of Inorganic Biochemistry.* 2019;194:114–152.

6. Yusof ENM, Ravoof TBSA, Page AJ. Cytotoxicity of Tin(IV)-based compounds: A review. *Polyhedron.* 2021;198:115069.

7. Beck M. *Mesoporöse Silikananopartikel als Transportsysteme für miRNA und Wirkstoffmoleküle für die Therapie von Krebsstammzellen*. Universität Ulm, 2018.

8. Nam L, Coll C, Erthal LCS, La Torre C de, Serrano D, Martínez-Máñez R, Santos-Martínez MJ, Ruiz-Hernández E. Drug Delivery Nanosystems for the Localized Treatment of Glioblastoma Multiforme. *Materials.* 2018;11(5).

9. Frickenstein AN, Hagood JM, Britten CN, Abbott BS, McNally MW, Vopat CA, Patterson EG, MacCuaig WM, Jain A, Walters KB, McNally LR. Mesoporous Silica Nanoparticles: Properties and Strategies for Enhancing Clinical Effect. *Pharmaceutics.* 2021;13(4).

10. Predarska I, Saoud M, Morgan I, Eichhorn T, Kaluđerović GN, Hey-Hawkins E. Cisplatin-cyclooxygenase inhibitor conjugates, free and immobilised in mesoporous silica SBA-15, prove highly potent against triple-negative MDA-MB-468 breast cancer cell line. *Dalton Transactions.* 2022;51(3):857–869.

11. Mamaeva V, Sahlgren C, Lindén M. Mesoporous silica nanoparticles in medicine--recent advances. *Advanced Drug Delivery Reviews.* 2013;65(5):689–702.

12. Lu J, Liong M, Li Z, Zink JI, Tamanoi F. Biocompatibility, biodistribution, and drug-delivery efficiency of mesoporous silica nanoparticles for cancer therapy in animals. *Small.* 2010;6(16):1794–1805.

13. Gao Y, Gao D, Shen J, Wang Q. A Review of Mesoporous Silica Nanoparticle Delivery Systems in Chemo-Based Combination Cancer Therapies. *Frontiers in Chemistry.* 2020;8:598722.

14. Watermann AEK. *Evaluation of Mesoporous Silica Nanoparticles for Head and Neck Cancer Therapy.* Johannes Gutenberg-Universität Mainz, 2019.

15. Tao Z, Toms B, Goodisman J, Asefa T. Mesoporous silica microparticles enhance the cytotoxicity of anticancer platinum drugs. *ACS nano.* 2010;4(2):789–794.

16. Asefa T, Tao Z. Biocompatibility of mesoporous silica nanoparticles. *Chemical Research in Toxicology.* 2012;25(11):2265–2284.

17. Lin Y-S, Haynes CL. Impacts of mesoporous silica nanoparticle size, pore ordering, and pore integrity on hemolytic activity. *Journal of the American Chemical Society.* 2010;132(13):4834–4842.

18. He Q, Zhang Z, Gao F, Li Y, Shi J. In vivo biodistribution and urinary excretion of mesoporous silica nanoparticles: effects of particle size and PEGylation. *Small.* 2011;7(2):271–280.

19. Gordon S. Phagocytosis: An Immunobiologic Process. *Immunity.* 2016;44(3):463–475.

20. Wongrakpanich S, Wongrakpanich A, Melhado K, Rangaswami J. A Comprehensive Review of Non-Steroidal Anti-Inflammatory Drug Use in The Elderly. *Aging and Disease.* 2018;9(1):143–150.

21. Buer JK. Origins and impact of the term 'NSAID'. *Inflammopharmacology.* 2014;22(5):263–267.

22. Ida Ghlichloo, Valerie Gerriets. Nonsteroidal Anti-inflammatory Drugs (NSAIDs). In: Ghlichloo I, Gerriets V, editors. *StatPearls [Internet].* StatPearls Publishing, 2021.

23. Kaduševičius E. Novel Applications of NSAIDs: Insight and Future Perspectives in Cardiovascular, Neurodegenerative, Diabetes and Cancer Disease Therapy. *International Journal of Molecular Sciences.* 2021;22(12).

24. Weinblatt ME. Anti-Inflammatory Drugs: NSAIDs, COX-2 Selective Inhibitors, Gluococorticoids and Anti-Cytokine Agents: Principles of Pharmacology. Lecture Notes., Spring. https://ocw.mit.edu/courses/health-sciences-and-technology/hst-151-principles-of-pharmacology-spring-2005/lecture-notes/0215_2_weinblatt.pdf.

25. Botting RM. Inhibitors of cyclooxygenases: mechanisms, selectivity and uses. *Journal of Physiology and Pharmacology.* 2006;57 Suppl 5:113–124.

26. Zuske-Matthäus A. *Die Expression der Cyclooxygenase-2 als unabhängiger prognostischer Faktor bei Tatienten mit malignen Lympohomen*. Inauguralissertation. Lübeck: Universität zu Lübeck, 2011.

27. Ohshima K, Sugihara M, Suzumiya J, Haraoka S, Kanda M, Shimazaki K, Katoh K, Kumagawa M, Kikuchi M. Basic Fibroblast Growth Factor and Fibrosis in Hodgkin's Disease. *Pathology - Research and Practice.* 1999;195(3):149–155.

28. Traa MX, Derry S, Moore RA. Single dose oral fenoprofen for acute postoperative pain in adults. *The Cochrane Database of Systematic Reviews.* 2011;(2):CD007556.

29. Marjanović M, Zorc B, Pejnović L, Zovko M, Kralj M. Fenoprofen and ketoprofen amides as potential antitumor agents. *Chemical Biology & Drug Design.* 2007;69(3):222–226.

30. Coussens LM, Werb Z. Inflammation and cancer. *Nature.* 2002;420(6917):860–867.

31. Majumder J, Yedoti P, Dastidar P. A supramolecular topical gel derived from a non-steroidal anti-inflammatory drug, fenoprofen, is capable of treating skin inflammation in mice. *Organic & Biomolecular Chemistry.* 2015;13(8):2300–2309.

32. Srinivasan M, Sudheer AR, Menon VP. Ferulic Acid: therapeutic potential through its antioxidant property. *Journal of Clinical Biochemistry and Nutrition.* 2007;40(2):92–100.

33. Batista R. Ferulic acid: Uses and Potential Applications of Ferulic Acid. In: *Ferulic acid: Antioxidant properties*:39–70.

34. Nile SH, Ko EY, Kim DH, Keum Y-S. Screening of ferulic acid related compounds as inhibitors of xanthine oxidase and cyclooxygenase-2 with anti-inflammatory activity. *Revista Brasileira de Farmacognosia.* 2016;26(1):50–55.

35. Kampa M, Alexaki V-I, Notas G, Nifli A-P, Nistikaki A, Hatzoglou A, Bakogeorgou E, Kouimtzoglou E, Blekas G, Boskou D, Gravanis A, Castanas E. Antiproliferative and

apoptotic effects of selective phenolic acids on T47D human breast cancer cells: potential mechanisms of action. *Breast Cancer Research : BCR.* 2004;6(2):R63-74.

36. Ip MS, Affordability. WHO model list of essential medicines - 22nd list, 2021. *World Health Organization.* 2021.

37. Amir MK, Khan S, Zia-ur-Rehman, Shah A, Butler IS. Anticancer activity of organotin(IV) carboxylates. *Inorganica Chimica Acta.* 2014;423:14–25.

38. Rehman W, Baloch MK, Badshah A. Synthesis, spectral characterization and bio-analysis of some organotin(IV) complexes. *European Journal of Medicinal Chemistry.* 2008;43(11):2380–2385.

39. Yamabe Y, Hoshino A, Imura N, Suzuki T, Himeno S. Enhancement of androgen-dependent transcription and cell proliferation by tributyltin and triphenyltin in human prostate cancer cells. *Toxicology and Applied Pharmacology.* 2000;169(2):177–184.

40. Díaz-García D, Cenariu D, Pérez Y, Cruz P, Del Hierro I, Prashar S, Fischer-Fodor E, Gómez-Ruiz S. Modulation of the mechanism of apoptosis in cancer cell lines by treatment with silica-based nanostructured materials functionalized with different metallodrugs. *Dalton Transactions.* 2018;47(35):12284–12299.

41. Pantelic N, Lerbs M, Wolf K, Wessjohann L, Kaludjerovic G. In vitro anticancer evaluation of novel triphenyltin(IV) compounds with some N-acetyl-S-naphthoquinonylcysteine derivatives. *Journal of the Serbian Chemical Society.* 2019;84(10):1119–1127.

42. Bulatović MZ, Maksimović-Ivanić D, Bensing C, Gómez-Ruiz S, Steinborn D, Schmidt H, Mojić M, Korać A, Golić I, Pérez-Quintanilla D, Momčilović M, Mijatović S, Kaluđerović GN. Organotin(IV)-loaded mesoporous silica as a biocompatible strategy in cancer treatment. *Angewandte Chemie International ed.* 2014;53(23):5982–5987.

43. Maksimović-Ivanić D, Bulatović M, Edeler D, Bensing C, Golić I, Korać A, Kaluđerović GN, Mijatović S. The interaction between SBA-15 derivative loaded with Ph3Sn(CH2)6OH and human melanoma A375 cell line: uptake and stem phenotype loss. *Journal of Biological Inorganic Chemistry.* 2019;24(2):223–234.

44. Buddrus J. *Grundlagen der organischen Chemie* (2019th edition). Berlin, Boston: De Gruyter, 2020.

45. Steinborn D. *Grundlagen der metallorganischen Komplexkatalyse*. Berlin, Heidelberg: Springer Berlin Heidelberg, 2019.

46. Gómez-Ruiz S, Ceballos-Torres J, Prashar S, Fajardo M, Žižak Ž, Juranić ZD, Kaluđerović GN. One ligand different metal complexes: Biological studies of titanium(IV), tin(IV) and gallium(III) derivatives with the 2,6-dimethoxypyridine-3-carboxylato ligand. *Journal of Organometallic Chemistry.* 2011;696(20):3206–3213.

47. Gómez-Ruiz S, Kaluderović GN, Prashar S, Hey-Hawkins E, Erić A, Zizak Z, Juranić ZD. Study of the cytotoxic activity of di and triphenyltin(IV) carboxylate complexes. *Journal of Inorganic Biochemistry.* 2008;102(12):2087–2096.

48. Kaluđerović GN, Kommera H, Hey-Hawkins E, Paschke R, Gómez-Ruiz S. Synthesis and biological applications of ionic triphenyltin(IV) chloride carboxylate complexes with exceptionally high cytotoxicity. *Metallomics: Integrated Biometal Science.* 2010;2(6):419–428.

49. Romero-Chávez MM, Pineda-Urbina K, Pérez DJ, Obledo-Benicio F, Flores-Parra A, Gómez-Sandoval Z, Ramos-Organillo Á. Organotin(IV) compounds derived from ibuprofen and cinnamic acids, an alternative into design of anti-inflammatory by the cyclooxygenases (COX-1 and COX-2) pathway. *Journal of Organometallic Chemistry.* 2018;862:58–70.

50. PubChem. Hazardous Substances Data Bank (HSDB) : 5689. 2021. https://pubchem.ncbi.nlm.nih.gov/source/hsdb/5689#section=Density. [Accessed 15 December 2021].

51. Touaibia M, Guay M. Natural Product Total Synthesis in the Organic Laboratory: Total Synthesis of Caffeic Acid Phenethyl Ester (CAPE), A Potent 5-Lipoxygenase Inhibitor from Honeybee Hives. *Journal of Chemical Education.* 2011;88(4):473–475.

52. Friebolin H. *Ein- und zweidimensionale NMR-Spektroskopie: Eine Einführung* (5th edition). Weinheim: Wiley-VCH, 2013.

53. Vogeli U, Philipsborn W von. Vicinal C,H spin coupling in substituted alkenes. Stereochemical significance and structural effects. *Organic Magnetic Resonance.* 1975;7(12):617–627.

54. Maciel GE, McIver JW, Ostlund NS, Pople JA. Approximate self-consistent molecular orbital theory of nuclear spin coupling. IV. Vicinal proton-proton coupling constants in

substituted ethanes and ethylenes and related compounds. *Journal of the American Chemical Society.* 1970;92(15):4497–4506.

55. Ng S, Sathasivam RV, Lo KM. Possible intermolecular association in triphenyltin chloride in the solution state as detected by NMR spectroscopy. *Magnetic Resonance in Chemistry : MRC.* 2011;49(11):749–752.

56. Holeček J, Handlíř K, Nádvorník M, Lyčka A. 13C and 119Sn NMR study of some triphenyltin(IV) carboxylates. *Journal of Organometallic Chemistry.* 1983;258(2):147–153.

57. Pellerito C, Emanuele S, Ferrante F, Celesia A, Giuliano M, Fiore T. Tributyltin(IV) ferulate, a novel synthetic ferulic acid derivative, induces autophagic cell death in colon cancer cells: From chemical synthesis to biochemical effects. *Journal of Inorganic Biochemistry.* 2020;205:110999.

58. Holeček J, Nádvorník M, Handlíř K, Lyčka A. 13C and 119Sn NMR Study of some four- and five-coordinate triphenyltin(IV) compounds. *Journal of Organometallic Chemistry.* 1983;241(2):177–184.

59. Basu Baul TS, Singh KS, Holčapek M, Jirásko R, Rivarola E, Linden A. Synthesis, characterization and crystal structures of polymeric and dimeric triphenyltin(IV) complexes of 4-[((E)-1-{2-hydroxy-5-[(E)-2-(2-carboxyphenyl)-1-diazenyl]phenyl}methylidene)amino]aryls. *Journal of Organometallic Chemistry.* 2005;690(19):4232–4242.

60. Basu Baul TS, Masharing C, Basu S, Rivarola E, Holčapek M, Jirásko R, Lyčka A, Vos D de, Linden A. Synthesis, characterization, cytotoxic activity and crystal structures of tri- and di-organotin(IV) complexes constructed from the β-{[(E)-1-(2-hydroxyaryl)alkylidene]amino}propionate and β-{[(2Z)-(3-hydroxy-1-methyl-2-butenylidene)]amino}propionate skeletons. *Journal of Organometallic Chemistry.* 2006;691(5):952–965.

61. Kumari R, Banerjee S, Roy P, Nath M. Organotin(IV) complexes of NSAID, ibuprofen, X-ray structure of Ph 3 Sn(IBF), binding and cleavage interaction with DNA and in vitro cytotoxic studies of several organotin complexes of drugs. *Applied Organometallic Chemistry.* 2020;34(1).

62. Wu S-H, Mou C-Y, Lin H-P. Synthesis of mesoporous silica nanoparticles. *Chemical Society Reviews.* 2013;42(9):3862–3875.

63. Castillo RR, La Torre L de, García-Ochoa F, Ladero M, Vallet-Regí M. Production of MCM-41 Nanoparticles with Control of Particle Size and Structural Properties: Optimizing Operational Conditions during Scale-Up. *International Journal of Molecular Sciences.* 2020;21(21).

64. Castillo RR, La Torre L de, García-Ochoa F, Ladero M, Vallet-Regí M. Production of MCM-41 Nanoparticles with Control of Particle Size and Structural Properties: Optimizing Operational Conditions during Scale-Up. *International Journal of Molecular Sciences.* 2020;21(21).

65. Thommes M, Kaneko K, Neimark AV, Olivier JP, Rodriguez-Reinoso F, Rouquerol J, Sing KSW. Physisorption of gases, with special reference to the evaluation of surface area and pore size distribution (IUPAC Technical Report). *Pure and Applied Chemistry.* 2015;87(9-10):1051–1069.

66. Schmidt R, Stöcker M, Hansen E, Akporiaye D, Ellestad OH. MCM-41: a model system for adsorption studies on mesoporous materials. *Microporous Materials.* 1995;3(4-5):443–448.

67. Miricioiu MG, Iacob C, Nechifor G, Niculescu V-C. High Selective Mixed Membranes Based on Mesoporous MCM-41 and MCM-41-NH2 Particles in a Polysulfone Matrix. *Frontiers in Chemistry.* 2019;7:332.

68. Vallet-Regi M, Rámila A, del Real RP, Pérez-Pariente J. A New Property of MCM-41: Drug Delivery System. *Chemistry of Materials.* 2001;13(2):308–311.

69. Vazquez NI, Gonzalez Z, Ferrari B, Castro Y. Synthesis of mesoporous silica nanoparticles by sol–gel as nanocontainer for future drug delivery applications. *Boletín de la Sociedad Española de Cerámica y Vidrio.* 2017;56(3):139–145.

70. Dhal JP, Dash T, Hota G. Iron oxide impregnated mesoporous MCM-41: synthesis, characterization and adsorption studies. *Journal of Porous Materials.* 2020;27(1):205–216.

71. Schoeffel M, Brodie–Linder N, Audonnet F, Alba–Simionesco C. Wall thickness determination of hydrophobically functionalized MCM-41 materials. *Journal of Materials Chemistry.* 2012;22(2):557–567.

6. Appendix
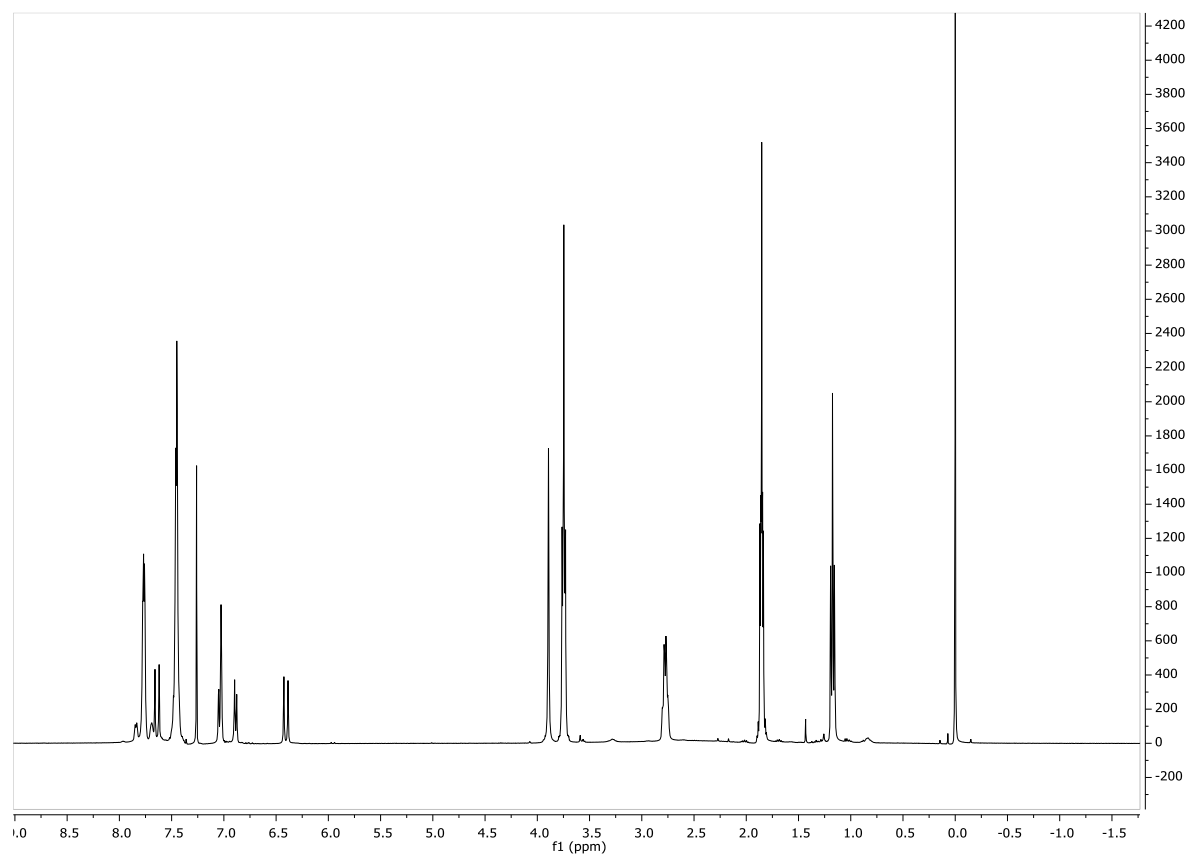
Figure A 1: ^1H NMR of [Ph$_3$Sn(fa)]) before extraction with DCM/water, in CDCl$_3$
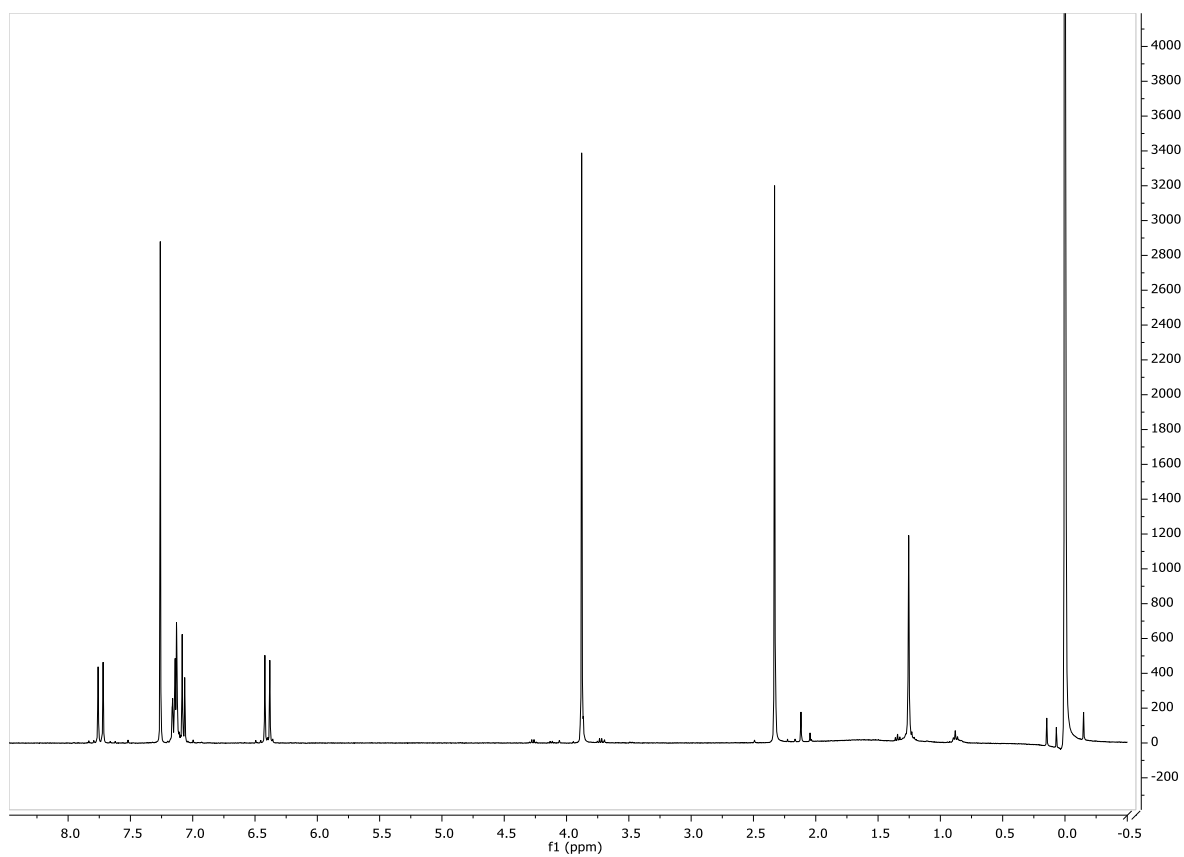
Figure A 2: ^{1}H NMR spectrum of Acfa, in CDCl$_3$
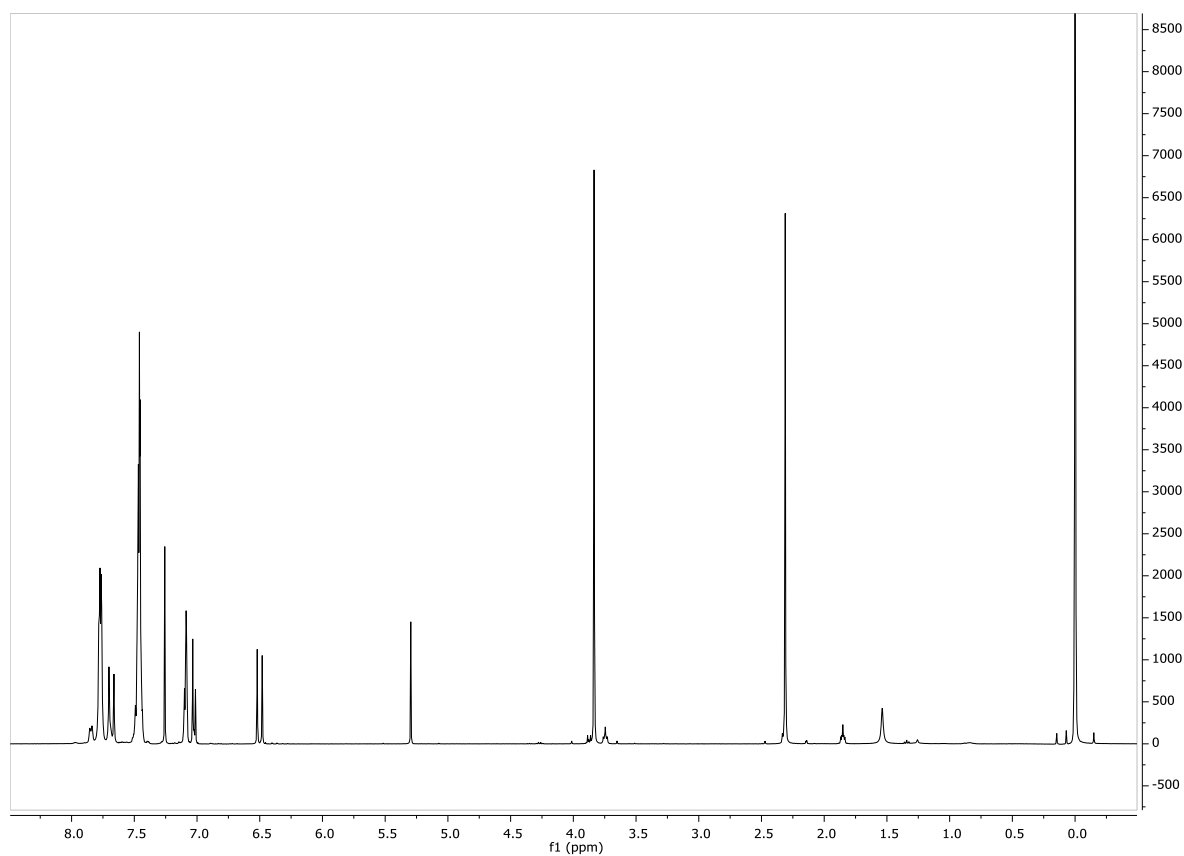
Figure A 3: ^{1}H NMR spectrum of [Ph$_3$Sn(Acfa)], in CDCl$_3$
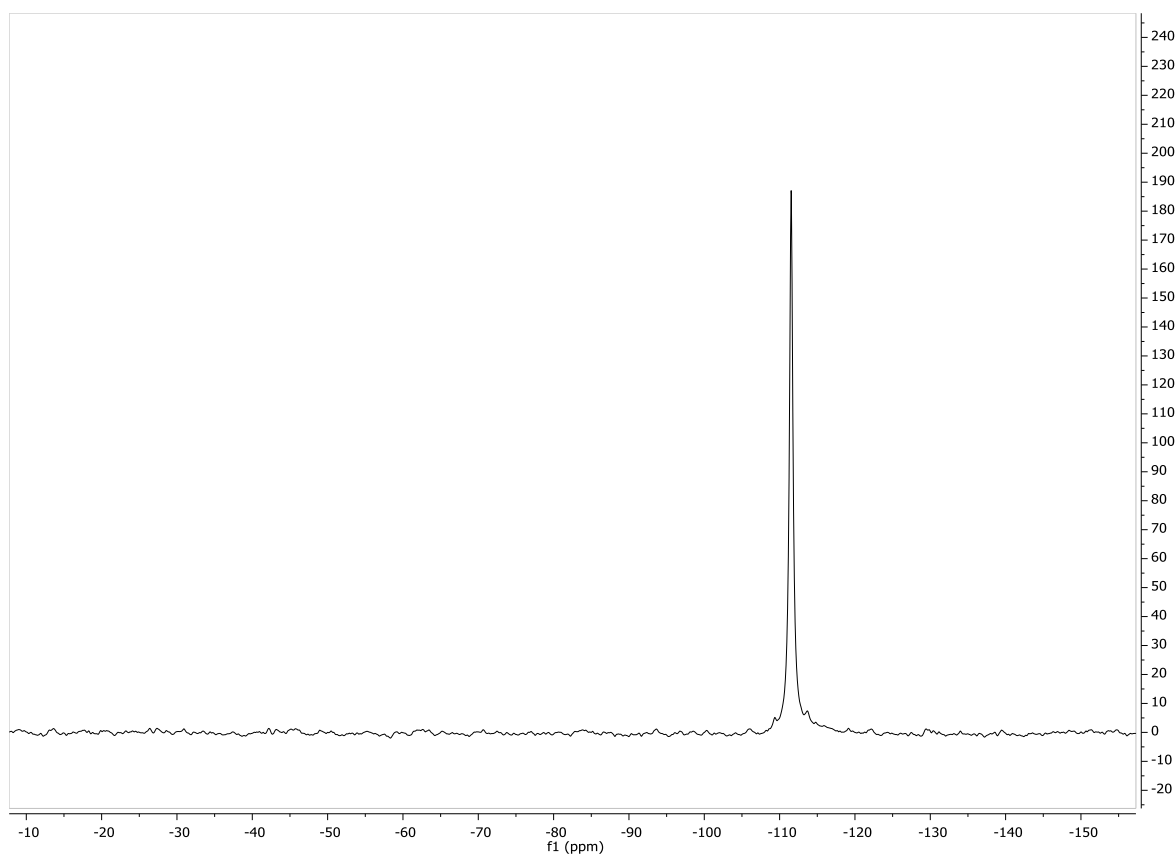
Figure A 4: ^{119}Sn NMR of [Ph₃Sn(Acfe)], in CDCl₃
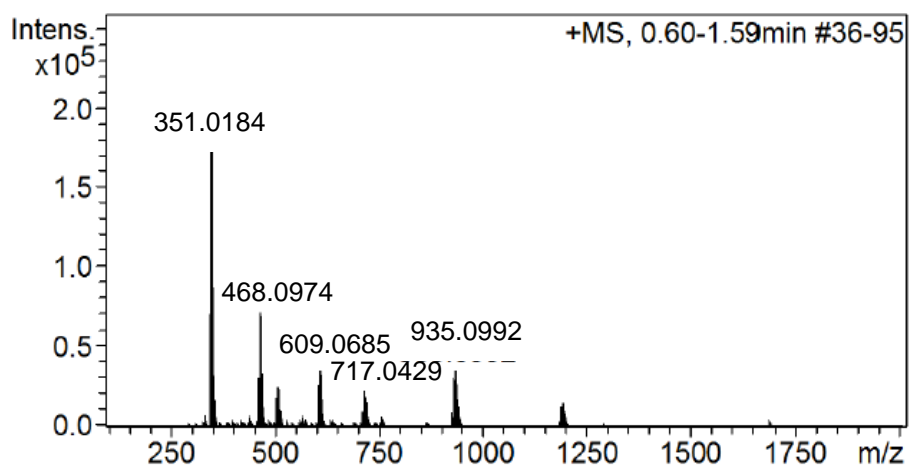
Figure A 5: HR-ESI-MS of [Ph₃Sn(Acfe)] in positive mode
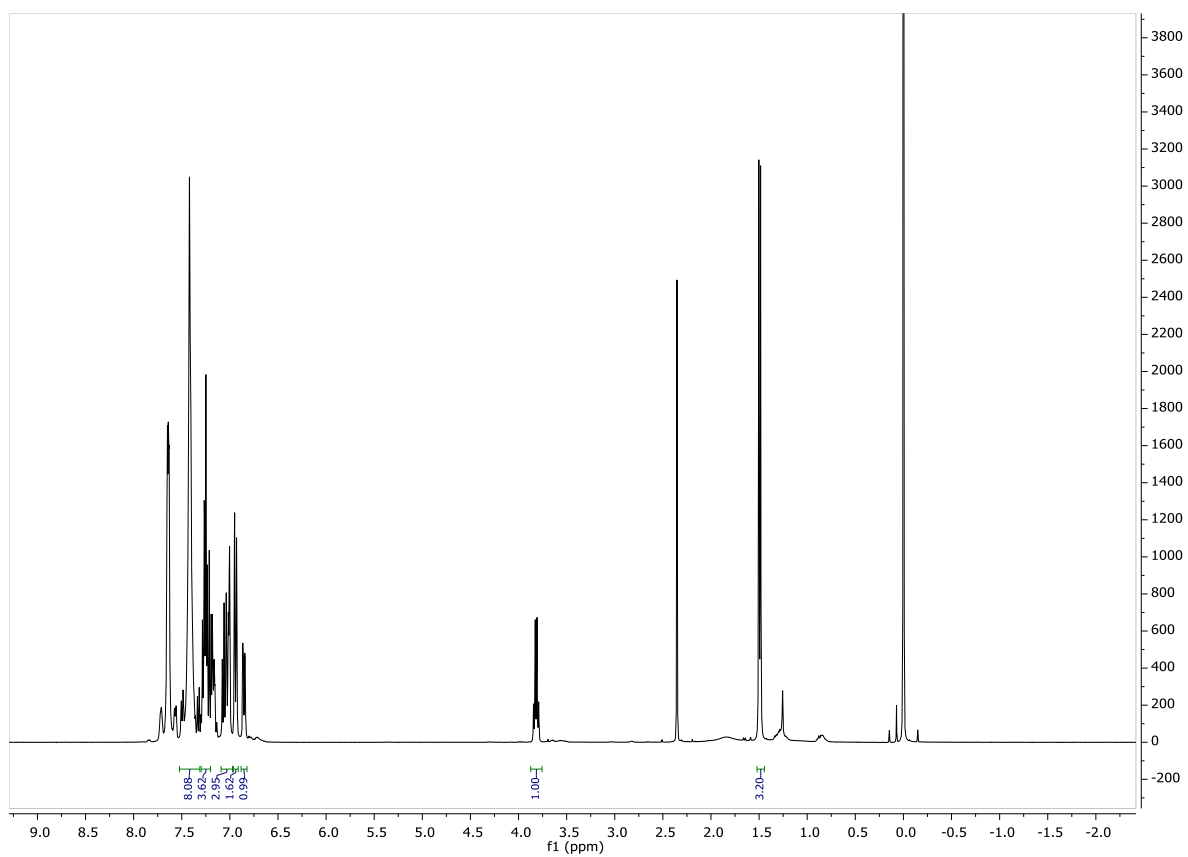
Figure A 6: ^{1}H NMR spectrum of [Ph$_3$Sn(fen)], in CDCl$_3$
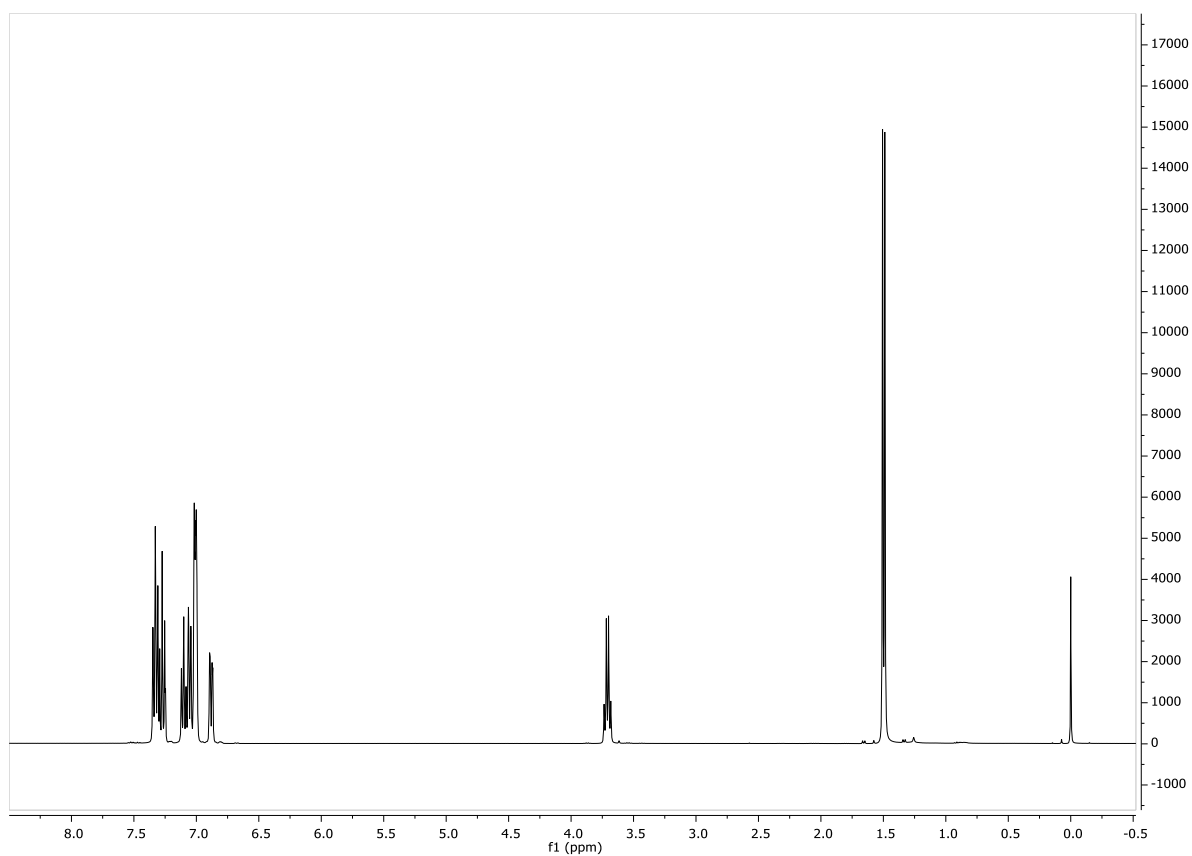
Figure A 7: ^{1}H NMR spectrum of fen, in CDCl$_3$

47
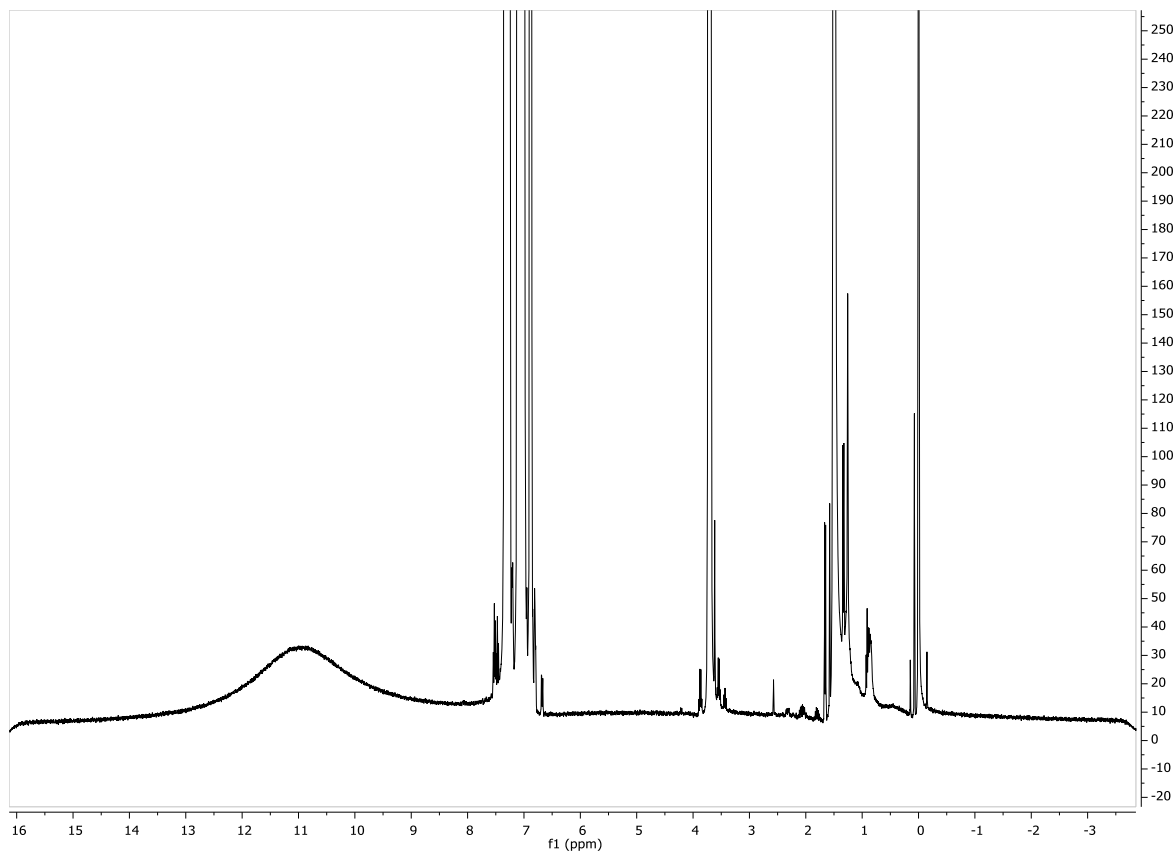
Figure A 8: ^1H NMR spectrum of fen with acidic proton, in CDCl$_3$
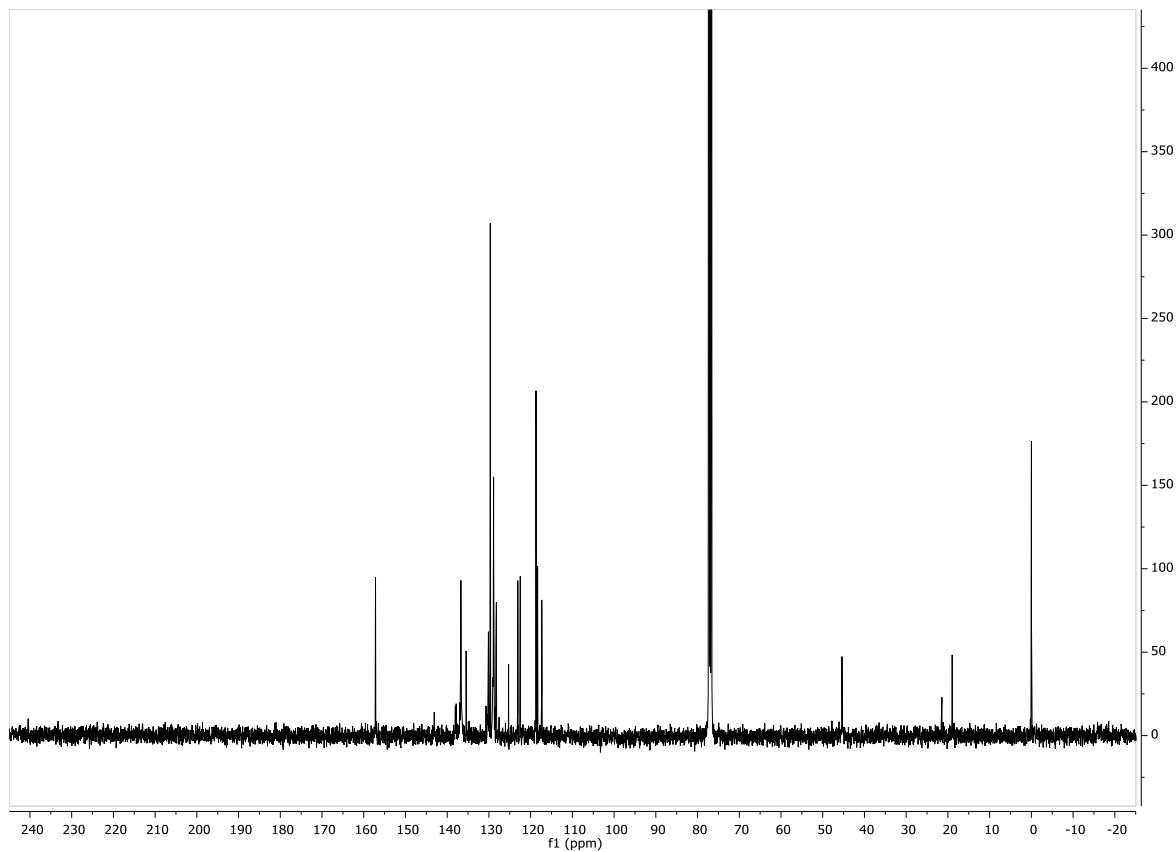
Figure A 9: ^{13}C NMR spectrum of [Ph$_3$Sn(fen)], in CDCl$_3$

48
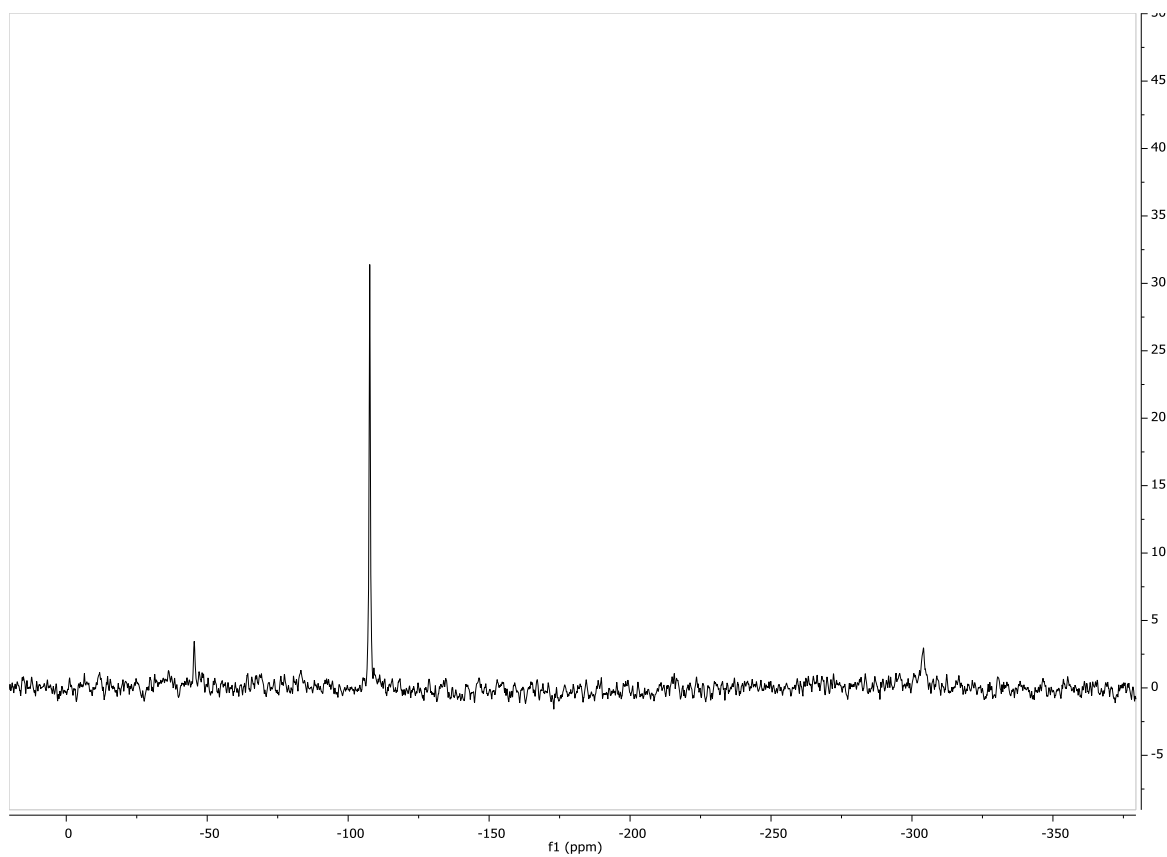
Figure A 10: ^{119}Sn NMR spectrum of [Ph$_3$Sn(fen)], in CDCl$_3$
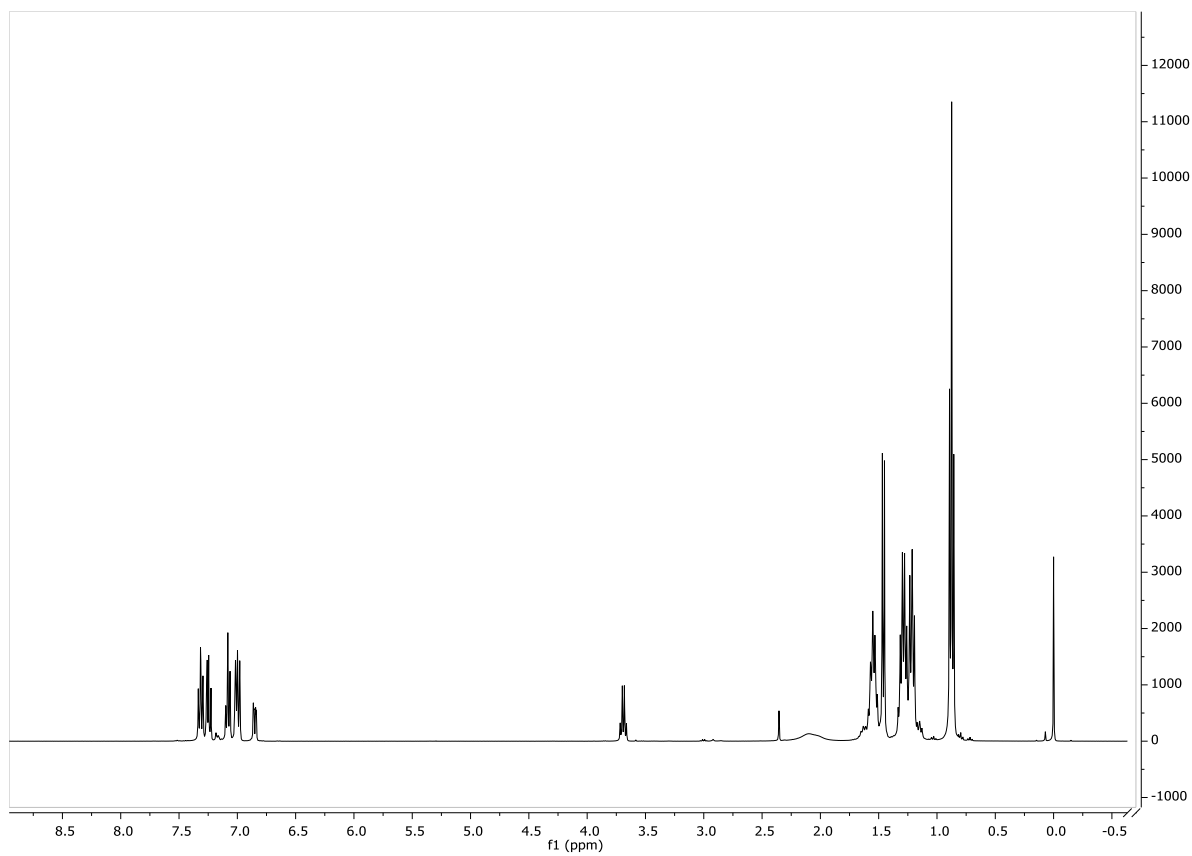
Figure A 11: ^1H NMR of [Bu$_3$Sn(fen)], in CDCl$_3$

49
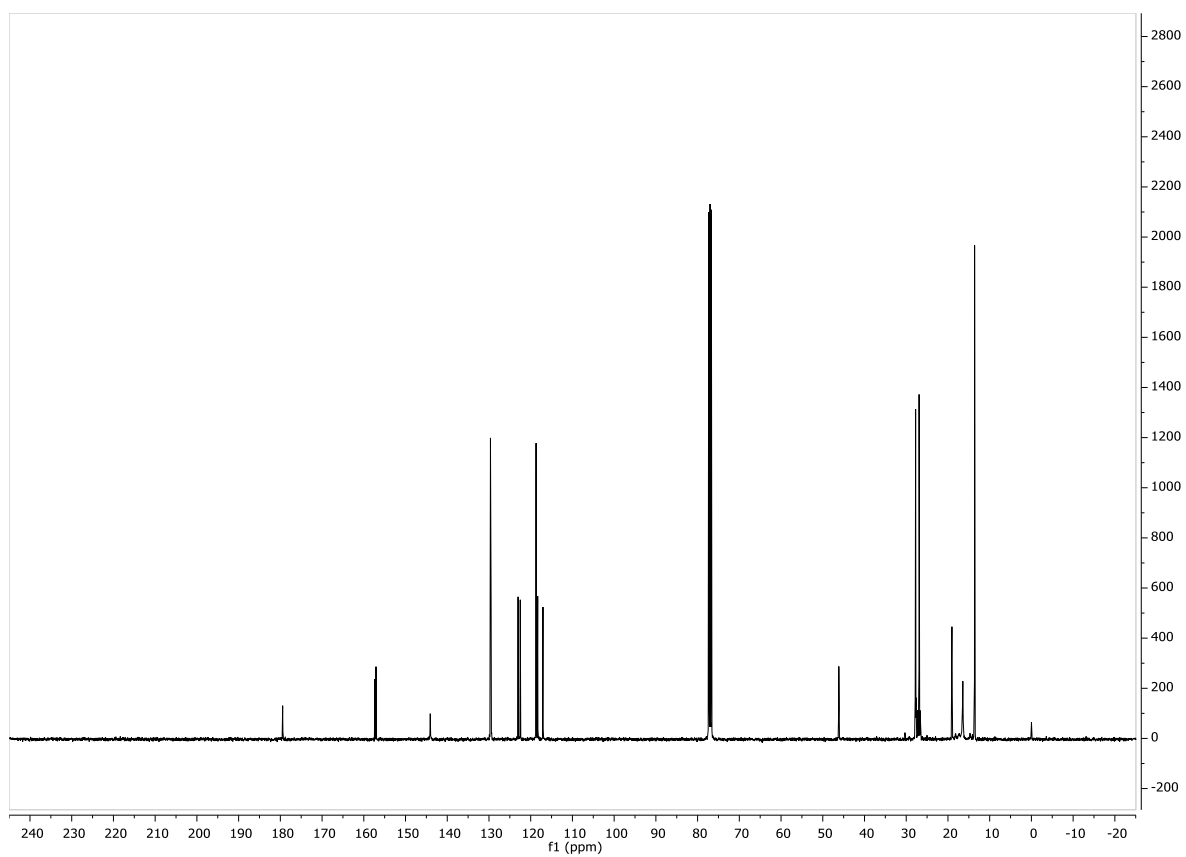
Figure A 12: ^{13}C NMR of [Bu$_3$Sn(fen)], in CDCl$_3$
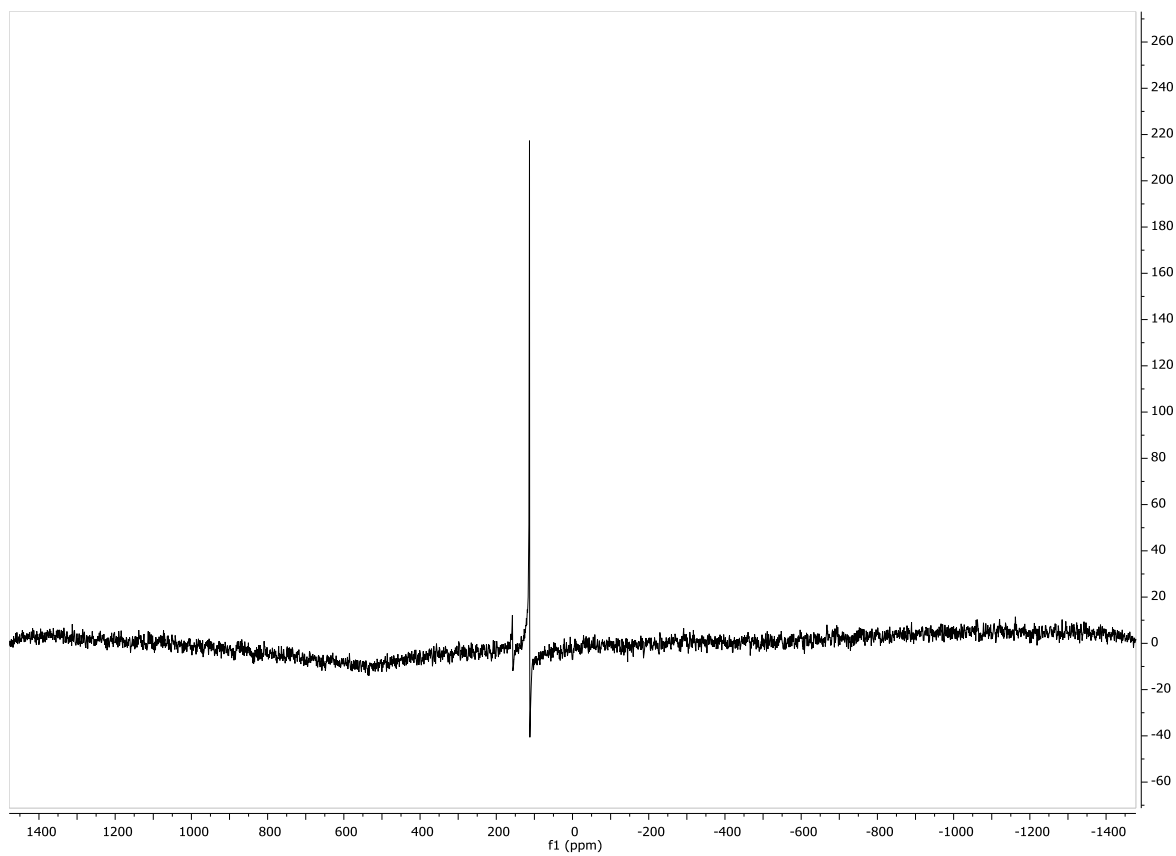
Figure A 13: ^{119}Sn NMR of [Bu$_3$Sn(fen)], in CDCl$_3$
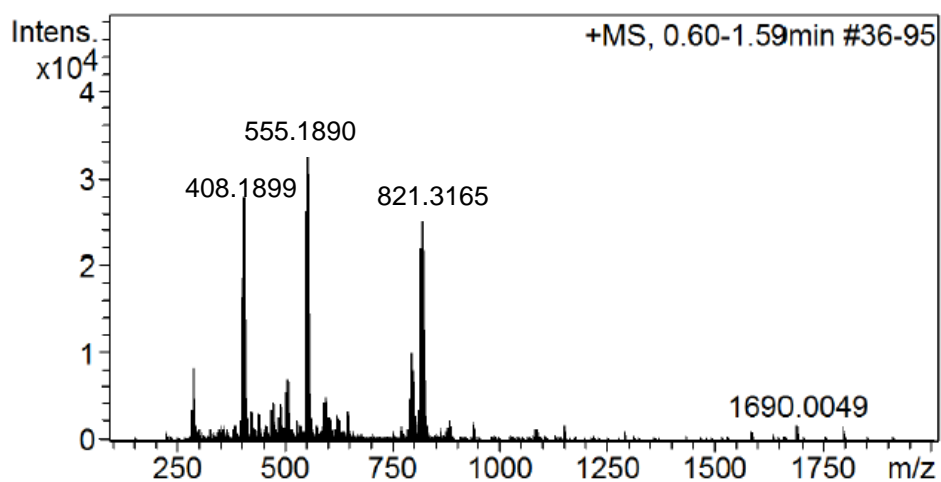
Figure A 14: HR-ESI-MS of [Bu₃Sn(fen)] in positive mode
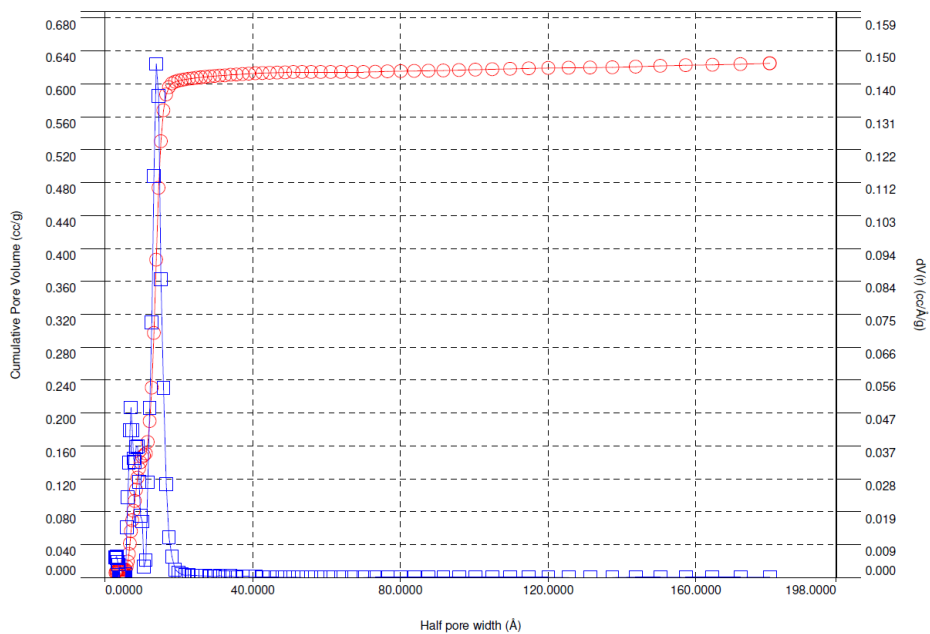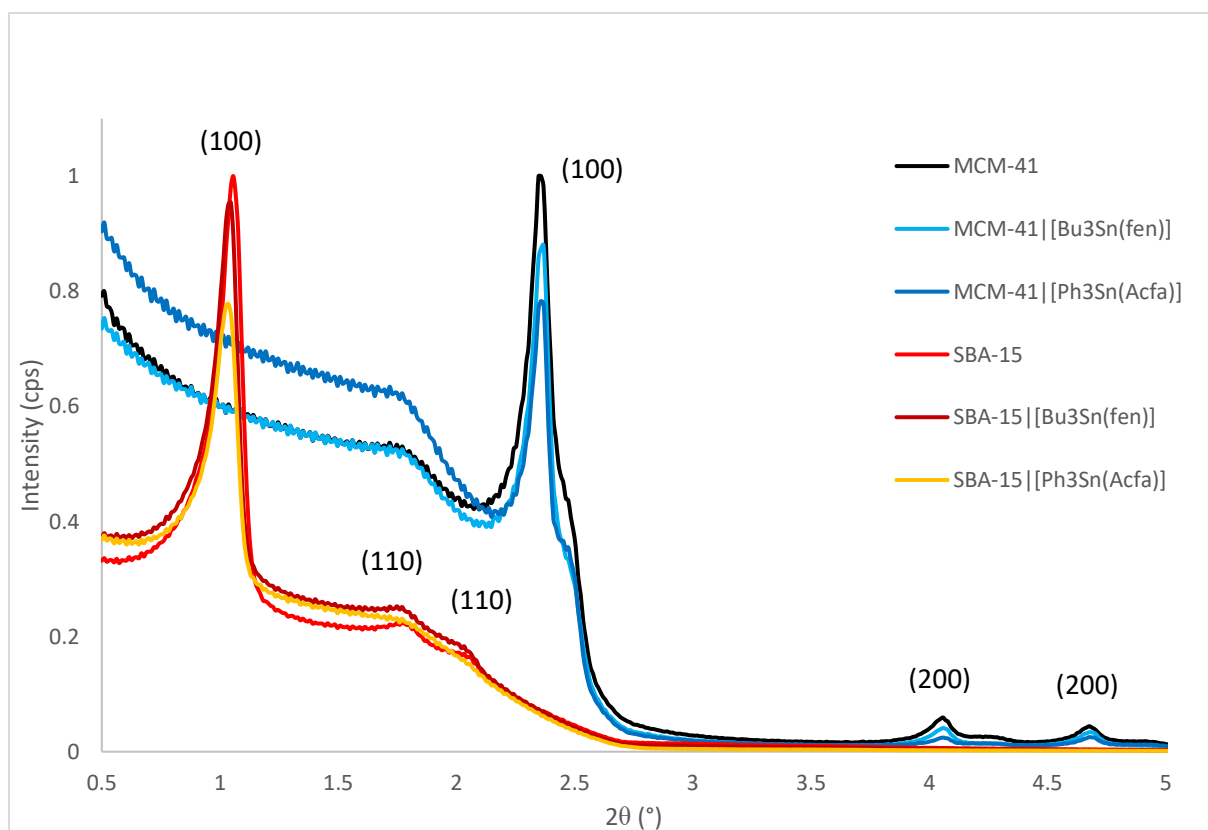

Figure A 15: DFT pore size distribution for MCM-41

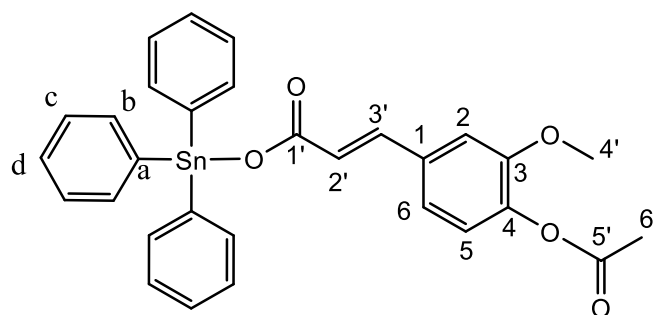*Figure A 16: SAXS results for pure and compound-loaded MSNs*

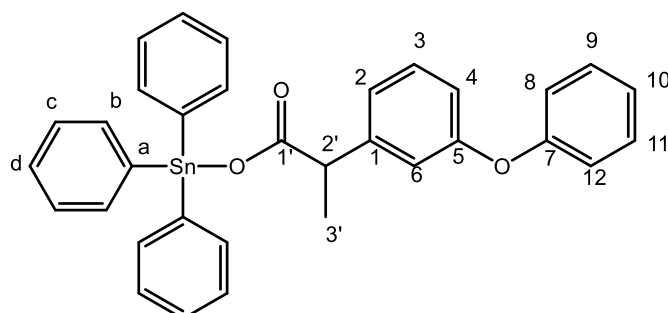*Figure A 17: Structure of (4-*O*-acetyl ferulato)triphenyltin(IV)*

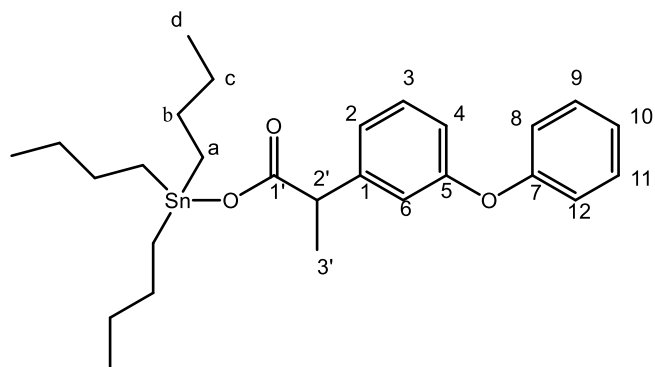*Figure A 18: Structure of (fenoprofenato)triphenyltin(IV)*

Figure A 19: Structure of (fenoprofenato)tributyltin(IV)